Draft version February 19, 2016
Preprint typeset using LaTeX style emulateapj v. 5/2/11

arXiv:1601.01691v2 [astro-ph.GA] 17 Feb 2016

THE H I CONTENT OF THE UNIVERSE OVER THE PAST 10 GYRS

Marcel Neeleman[1,2,3], J. Xavier Prochaska[2], Joseph Ribaudo[4], Nicolas Lehner[5],J. Christopher Howk[5],Marc Rafelski[6], Nissim Kanekar[7]

Draft version February 19, 2016

ABSTRACT

We use the Hubble Space Telescope (HST) archive of ultraviolet (UV) quasar spectroscopy to conduct the first blind survey for damped Ly-α absorbers (DLAs) at low redshift ($z < 1.6$). Our statistical sample includes 463 quasars with spectral coverage spanning a total redshift path $\Delta z = 123.3$ or an absorption path $\Delta X = 229.7$. Within this survey path, we identify 4 DLAs defined as absorbers with H I column density $N_{\rm HI} \geq 10^{20.3}\,{\rm cm}^{-2}$, which implies an incidence per absorption length $\ell_{\rm DLA}(X) = 0.017^{+0.014}_{-0.008}$ at a median survey path redshift of $z = 0.623$. While our estimate of $\ell_{\rm DLA}(X)$ is lower than earlier estimates at $z \approx 0$ from H I 21 cm emission studies, the results are consistent within the measurement uncertainties. Our dataset is too small to properly sample the $N_{\rm HI}$ frequency distribution function $f(N_{\rm HI}, X)$, but the observed distribution agrees with previous estimates at $z > 2$. Adopting the $z > 2$ shape of $f(N_{\rm HI}, X)$, we infer an H I mass density at $z \sim 0.6$ of $\rho_{\rm HI}^{\rm DLA} = 0.25^{+0.20}_{-0.12} \times 10^8 M_\odot {\rm Mpc}^{-3}$. This is significantly lower than previous estimates from targeted DLA surveys with the HST, but consistent with results from low-z H I 21 cm observations, and suggests that the neutral gas density of the universe has been decreasing over the past 10 Gyrs.

Subject headings: galaxies: evolution — intergalactic medium — galaxies: ISM — ISM: evolution — quasars: absorption lines

1. INTRODUCTION

Galaxy formation and evolution are critically dependent on the gas within and surrounding a galaxy. As galaxies evolve, gas is accreted onto the galaxy and expelled through various processes such as activity of an active galactic nucleus and stellar feedback. Providing observational constraints on this gas is therefore paramount in understanding how galaxies formed and evolved. At very low redshifts, neutral gas has been studied in detail using the H I 21 cm line. Unfortunately, such observations are limited with current facilities to very low redshifts, $z \lesssim 0.25$ (e.g., Zwaan et al. 2001; Catinella et al. 2008; Fernández et al. 2013; Catinella & Cortese 2015).

To study how the mass and distribution of neutral gas has evolved over cosmic time, we need to measure the cosmic density of this gas over a large redshift range. Such a study can be done by studying the gas through Ly-α absorption in quasar spectra (Wolfe et al. 1986). Previous studies have shown that the highest column density absorbers, the damped Ly-α systems (DLAs), which have neutral hydrogen column densities of $N_{\rm HI} \geq 10^{20.3}\,{\rm cm}^{-2}$, contain the bulk of the neutral gas at both low and high redshifts (e.g., Prochaska et al. 2005; Wolfe et al. 2005; Zwaan et al. 2005; O'Meara et al. 2007). Observations of DLAs therefore provide an excellent opportunity to constrain the neutral hydrogen content of our Universe over a large redshift range.

To quantify the overall H I content of our Universe, we use a single quantity known as the neutral hydrogen column density distribution function, $f(N_{\rm HI}, X)$, (e.g., Tytler 1987; Lanzetta et al. 1991; Prochaska et al. 2005). $f(N_{\rm HI}, X)$ is a quantitative description of the large scale neutral hydrogen distribution of our Universe, and its zeroth and first moment yield the line density of DLAs, $\ell_{\rm DLA}(X)$, and the total hydrogen mass density of the Universe, $\rho_{\rm HI}^{\rm DLA}$.

At high redshifts, $z \gtrsim 2$, $f(N_{\rm HI}, X)$ for DLAs has been measured by many authors (e.g., Prochaska & Wolfe 2009; Noterdaeme et al. 2012; but see Crighton et al. 2015 and Sánchez-Ramírez et al. 2015), using large optical surveys such as the Sloan Digital Sky Survey (SDSS; Abazajian et al. 2009). These studies find that the shape of $f(N_{\rm HI}, X)$ is invariant between $z \sim 2$ and $z \sim 3.5$, while the normalization is observed to evolve, decreasing by a factor of $\approx 1.3 - 2$. This implies a concomitant decrease in $\ell_{\rm DLA}(X)$ and $\rho_{\rm HI}^{\rm DLA}$. Such evolution may be explained by either gas conversion into stars over this redshift range or feedback processes that expel gas from galaxies (e.g., Prochaska & Wolfe 2009).

A key feature of $f(N_{\rm HI}, X)$ and its moments is that they appear to converge by $z \sim 2$ to the present-day values estimated using H I 21 cm studies (Zwaan et al. 2005; Braun 2012; Delhaize et al. 2013; Hoppmann et al. 2015). This suggests that these quantities have remained essentially unchanged over the last 10 billion years of galaxy evolution. Unfortunately, at $z \lesssim 2$, it is difficult to measure $f(N_{\rm HI}, X)$ directly, because the effectiveness of optical surveys plummets due to the atmospheric absorption of ultraviolet (UV) radiation (Lanzetta et al. 1995).

[1] Department of Physics and Center for Astrophysics and Space Sciences, UCSD, La Jolla, CA 92093, USA
[2] Department of Astronomy & Astrophysics, UCO/Lick Observatory, 1156 High Street, University of California, Santa Cruz, CA 95064, USA
[3] marcel@ucsc.edu
[4] Department of Physics, Utica College, 1600 Burrstone Road, Utica, NY 13502
[5] Department of Physics, University of Notre Dame, Notre Dame, IN 46556
[6] NASA Postdoctoral Program Fellow, Goddard Space Flight Center, Code 665, Greenbelt, MD 20771, USA
[7] National Centre for Radio Astrophysics, Tata Institute of Fundamental Research, Pune University, Pune 411007, India

Table 1
QSO sample

QSO	$z_{\rm em}$ [a]	Instrument	Grating	Search Path			Statistical Path			Proposal ID
				$F_{\rm search}$ [b]	Min z	Max z	$F_{\rm stat}$ [c]	Min z	Max z	
J0000−1245	0.200	COS	G130M-G160M	1	0.010	0.299	1	0.010	0.188	12604
J0001+0709	3.234	STIS	G230L	1	—	—	0	—	—	8569
J0004−4157	2.760	FOS	G270H	1	1.501	1.695	0	—	—	6577
J0005+0524	1.900	FOS	G270H-G190H	1	0.829	1.695	1	0.829	1.695	4581,6705
J0005−5006	0.033	COS	G130M-G160M	1	0.010	0.133	1	0.010	0.022	12936

Note. — (Omitted from this portion of the table for brevity are the columns for alternate QSO name, right ascension and declination. These columns and the table in its entirety is available as a machine-readable table in the online journal. The complete sample table is also listed at the end of this manuscript minus the aforementioned columns.)

[a] Emission redshift of quasar.
[b] Search flag: (0) Low S/N or bad spectrum; (1) Included; (2) BAL quasar.
[c] Statistical flag: (0) Non-Statistical; (1) Statistical; (2) Galaxy Sample.

This problem can be circumvented by observing from space with the UV spectrographs on the Hubble Space Telescope (HST). However, due to the expense of these observations and the scarcity of DLAs in random lines of sight, large-scale blind surveys comparable to the SDSS have not been feasible within the limited time allocations of single observing programs.

To increase the rate of detection of high H I column density absorbers along quasar sightlines, previous studies at $z < 2$ have used several types of pre-selection methods, with the most common approach being the use of strong Mg II absorption to pre-select DLA and H I 21 cm candidates (e.g., Briggs & Wolfe 1983; Rao & Turnshek 2000; Rao et al. 2006; Kanekar et al. 2009). At redshifts $z \gtrsim 0.1$, the Mg II doublet is shifted into the optical regime. As the vast majority of DLAs show strong Mg II absorption (rest equivalent width, $W_0^{\lambda 2796} > 0.5$ Å), preselecting quasars with strong Mg II absorption will significantly increase the detection rate of DLAs in the sample. However, it has not so far been straightforward to understand the biases in such pre-selections, which are critical to obtain accurate estimates of $f(N_{\rm HI}, X)$ for DLAs (e.g., Rao et al. 2006).

Fortunately, 20 years of HST observations with a variety of UV spectrographs have resulted in a large sample of observed quasars. As HST nears the end of its mission, the time has come to explore this large data set, and perform a study in the UV to evaluate $f(N_{\rm HI}, X)$, $\ell_{\rm DLA}(X)$ and $\rho_{\rm HI}^{\rm DLA}$ at $z < 1.6$, similar to earlier studies performed in the optical regime. In this paper, we use the HST spectroscopic archive to obtain a measurement of the above quantities between $z \sim 0.01$ and $z \sim 1.6$, covering the past 10 billion years of the Universe. The sample for this study is described in Section 2, and the method is described in Section 3. Our results are presented in Section 4 and discussed in Section 5. Throughout this paper we adopt an $(\Omega_{\rm M}, \Omega_\Lambda, h) = (0.3, 0.7, 0.7)$ cosmology.

2. SAMPLE SELECTION

To measure the amount of neutral hydrogen between $z \sim 0.01$ and $z \sim 1.6$, we have assembled a large sample of quasars observed with medium resolution spectrographs on the Hubble Space Telescope. Specifically, we performed a search of the HST archive for quasars observed with either the Space Telescope Imaging Spectrograph (STIS), the Faint Object Spectrograph (FOS) or the Cosmic Origins Spectrograph (COS). These instruments have gratings that provide enough spectral resolution for a high fidelity search for strong absorption line systems (see Table 2 and Section 3.1). We did not include the Goddard High Resolution Spectrograph (GHRS), as its spectral coverage is too small to provide a meaningful search path. In total, a sample of 878 quasars were observed with at least one of these instruments and gratings.

Table 2
Spectrographs

Spectrograph	Grating	Resolution [a]	Spectral Range [b] (Å)
COS	G130M	18000	1138 - 1466
	G160M	18000	1410 - 1774
FOS	G160L	300	1351 - 2511
	G130H	1400	1140 - 1606
	G190H	1400	1590 - 2311
	G270H	1400	2223 - 3277
STIS	G140L	1200	1120 - 1716
	G230L	700	1573 - 3158

[a] The median resolving power at the central wavelength.
[b] The median central wavelengths for the complete data set.

We will not outline the procedure here used to analyze the spectra. Instead, we refer the reader to the following papers that describe the reduction process in detail for each of the different instruments and gratings. The FOS G160L and STIS spectra reductions are described in Ribaudo et al. (2011). We note that the FOS G160L data were cut off at a wavelength of 1350 Å. This arbitrary cut-off does not affect the results in this paper (see Section 4). The reduction of the higher resolution FOS spectra is detailed in Bechtold et al. (2002). Finally, the analysis of the COS spectra is described in Thom et al. (2011) and Meiring et al. (2011).

The reduced spectra were compiled into a single list, and, for quasars with multiple observations with different instruments, the spectra were combined into a single spectrum. In cases of overlapping spectral coverage, the higher resolution spectrum was used. We visually confirmed the emission redshift, and the quality of the spectra for all the quasars. Several quasars are not included either due to too low S/N or bad spectra (99 quasars). We also exclude any quasars that exhibit strong broad absorption line (BAL) features (12 quasars). A total of 767 quasars satisfy the above criteria and form the sam-

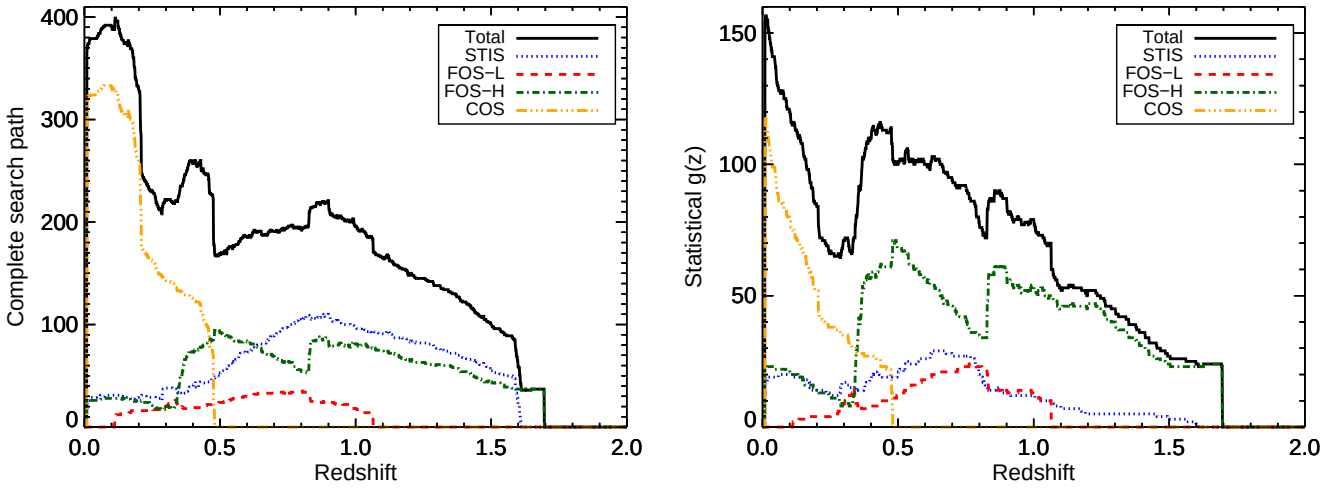

Figure 1. *Left panel:* The complete search path for our target sample of 767 quasars. The search paths of the individual spectrographs as well as the combined search path are plotted. *Right panel:* The statistical search path $g(z)$ for the statistical sample of quasars (i.e., those quasars with $f_{stat} = 1$). The total number of quasars included in this statistical sample is 463.

ple of this paper, as tabulated in Table 1.

2.1. *Statistical Sample*

To provide an accurate measurement of the H I column density distribution function, it is critical to provide an unbiased quasar sample, as the inclusion of quasar sightlines targeted to study known absorption systems would bias $f(N_{HI}, X)$ to higher values relative to the cosmic mean. Similarly, the inclusion of quasar sightlines that were targeted to contain a known absence of absorption systems would bias $f(N_{HI}, X)$ low. We have therefore carefully considered the stated selection criteria for each of the observed quasars. In Table 1, we have included a flag that indicates if the target quasar was observed for a bias with respect to the presence of an absorber along the sightline.

The statistical flag (f_{stat}) can take on three values. A flag of 0 indicates the observed quasar was targeted because it contained either an absorber (i.e., a known DLA or an Mg II system) or a lack of these systems along the line of sight. A flag of 1 indicates that the quasar was targeted independent of any known features along the line of sight. Finally a flag of 2 indicates that the quasar sightline crosses close to a previously recorded galaxy seen in emission. The true statistical sample defined in this paper contains only the targets with a statistical flag equal to 1, consisting of a total of 463 quasars. We also define an expanded sample in this paper which contains quasars with both $f_{stat} = 1$ and $f_{stat} = 2$ (677 quasars).

3. METHOD

To search for absorption systems in the HST spectra, we apply a method similar to that described in Prochaska et al. (2005), but slightly adapted for our lower redshift sample. Specifically, we define the search path for each quasar sightline, with the lower limit of the search path set by the signal-to-noise ratio (S/N) of the spectrum. We determine the S/N by calculating a running median with a 20-pixel width for each wavelength. The lower limit to the search path is set to the wavelength for which this median S/N is greater than the minimum allowed S/N, which we take to be 4, or the wavelength of Ly-α at $z = 0$ ($\lambda_{Ly\alpha} = 1215.6701$ Å), whichever is greater. The choice of 4 for this minimum S/N is explained in Section 3.2. The upper limit to the search path is set to be either the end of the spectrum or the value $(1 + z_{em} + \text{offset})\lambda_{Ly\alpha}$, whichever is smaller. Here, z_{em} is the quasar redshift; the redshift offset is added to allow absorption systems to have slightly higher redshifts than that of the quasar. This offset redshift (chosen to be 0.1) also encompasses the uncertainty in the reported quasar emission redshifts. The complete search path is shown in the left panel of Figure 1.

For those quasars that are part of the statistical sample, we also define a statistical search path, $g(z)$. The lower limit to the statistical path is set again by the wavelength where the median S/N exceeds the minimum S/N value of 4, or a wavelength of $(1+\text{offset})\lambda_{Ly\alpha}$, whichever is greater. This time, we adopt a redshift offset of 0.01 which is ~ 3000 km s^{-1} from our Galaxy. This offset is introduced to prevent any biasing due to clustering in the Milky Way neighborhood. The upper limit is set to the end of the spectrum or the value $\sqrt{(c-\Delta v)/(c+\Delta v)}(1+z_{em})\lambda_{Ly\alpha}$, whichever is greater. Here, Δv is taken to be 3000 km s^{-1} which prevents clustering around the quasar from affecting our measurements. The search path for the statistical sample ($f_{stat} = 1$) is shown in the right panel of Figure 1.

After defining the search path, we run our search algorithm to find candidate absorption systems along the search path to each quasar. The algorithm searches regions of the spectrum that fall below a specified S/N cut, which occurs in the absorption trough of strong absorbers. Specifically, the algorithm assigns to each pixel a DLA score, which is a measure of how many pixels in a 3 Å window centered around this pixel fall below the assigned S/N cut per pixel. We take a 3 Å window because this is the core width of a $N_{HI} = 10^{20.3}$ cm^{-2} absorber at $z = 0.01$, while the S/N threshold is taken to be 2. The central pixels for which greater than 60 % of the surrounding pixels in the 3 Å window fall below the

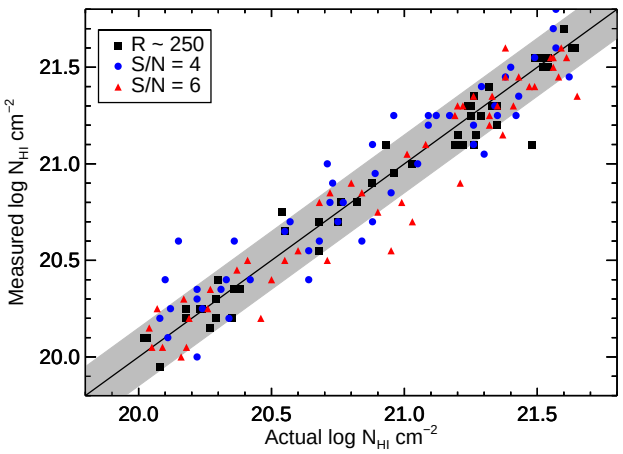

Figure 2. Results from various mock tests to quantify the effect of resolution and S/N on our ability to accurately determine the H I column density of individual absorbers, with the measured H I column density for simulated DLAs plotted versus their actual H I column density. The solid line indicates the case where the measured and actual H I column densities are equal, while the gray area marks the 0.15 dex range in dispersion around the actual value (the mean uncertainty that we have assigned to our fits). The fact that the measured H I column densities cluster around the solid line, with no systematic shifts, indicate that it is possible to obtain an accurate estimate of the H I column density for both low S/N ($\gtrsim 4$) and low resolution (R $\sim$ 250) data.

S/N threshold are flagged by the algorithm as candidate absorption systems. Altogether, we recorded 139 such candidates from the complete sample.

The final step in the search for absorption systems is the visual follow-up of these candidates. We fit individual absorption systems using a custom IDL Voigt-profile fitting program for DLAs, `x_fitdla`, which is part of the the publicly available IDL library, XIDL[8]. With this program, we are able to simultaneously fit both the Voigt profile and the continuum of the quasar as described in detail in Prochaska et al. (2003a). The largest source of uncertainty stems from the continuum placement.

As this process has inherently a human aspect to it, two of the authors (MN and JXP) independently carried out the fits to the candidate absorbers. The results were compared and, for most of the systems ($> 90\,\%$), the measured H I column density from both authors fell within the estimated 1-σ uncertainty of the measurement. We therefore believe that our column density measurements are robust.

3.1. *Resolution Considerations*

Low resolution spectra could result in inaccurate H I column density measurements and/or non-detection of DLAs by the search algorithm. Our lowest resolution spectra are taken with the low resolution gratings of the STIS G230L and FOS G160L, which have resolutions as low as R $\approx$ 250. For such resolutions, only about half of a resolution element falls within the DLA trough of a low column density system, and therefore small deviations could result in a non-detection of such a DLA by the search algorithm.

To assess the impact of resolution on the recovery process, we created simulated spectra with similar S/N and resolution to the observational data. We added artificial DLAs to the spectra with a range of column densities. For this mock data set, the algorithm was successful in recovering greater than 99 % of all of the absorbers with a column density above $10^{20}\,\mathrm{cm}^{-2}$. We conclude that the resolution of the spectra is sufficient to accurately recover DLAs.

We also test our ability to recover correct H I column density measurements by adding DLAs to our lowest resolution spectra and fitting these DLAs with the fitting procedure described in Section 3. In particular, we added 50 DLAs with varying H I column densities to our lowest resolution spectra (i.e. both STIS and FOS-L) and measured their H I column densities via our fitting method. The results are shown in Figure 2. As can be seen from the figure, we are able to accurately recover the actual H I column density over the full range of input values, including the lowest column density systems. Furthermore, the lower resolution does not cause any systematic under- or over-estimate of the H I column density. The deviation around the actual value for this sample is 0.10 dex, which is comparable to the fit uncertainties (which have a mean of 0.15 dex) that we have assigned to the sample.

As a final test, we have reanalyzed the results in this paper with the lowest resolution spectra omitted from the sample, and find no significant difference in any of the result presented.

3.2. *S/N Considerations*

Similar to the resolution of a spectrum, the S/N of a spectrum could affect both the search algorithm's efficacy and ability to accurately measure the H I column density of the absorption system during the fitting process. In the case of the search algorithm, low S/N spectra will flag more false positives as more pixels will satisfy the S/N cut criteria. To prevent high rates of false positive detections, we therefore set the minimum S/N ratio to be 4 over a 20 Å window, which is 2-σ above the S/N cut of 2 per 3 Å utilized in the search algorithm.

We note that Noterdaeme et al. (2009b) found that DLAs could go undetected in the search algorithm, if they occur sufficiently blueward in the spectrum as their damping wings would keep the S/N below the S/N cut. We have visually checked all of the spectra and find no evidence that this effect is present in our sample, likely because of the decrease in Ly-α forest density of these low redshift quasar sightlines.

We also need to be able to accurately determine the H I column density of the absorption systems with these S/N cuts. To test this, we insert artificial absorption systems in the real spectra and increase the noise level to the required S/N values. The fitting results are displayed in Figure 2. As is clear from the figure, we are able to accurately determine the H I column density of systems down to S/N$\approx$ 4 for even the lowest resolution data in the sample. The dispersion of the measured values around the actual H I column density for a spectrum with S/N= 4 is 0.15 dex.

We therefore conclude that a S/N threshold of 4 provides the ideal balance between maximizing the search path length while still providing the ability to reliably determine the H I column density of all DLAs in the search path.

[8] `http://www.ucolick.org/~xavier/IDL/`

Table 3
DLA sample

QSO Name	Alternate QSO Name	F_{stat} [a]	This Work		Literature		References
			z_{abs}	$\log N_{HI}$ [cm^{-2}]	z_{abs}	$\log N_{HI}$ [cm^{-2}]	
J0021−0128		1	1.2420	20.55 ± 0.10	1.2412	20.50	2
J0051+0041		0	0.7420	20.60 ± 0.10	0.7400	20.40 ± 0.10	3
J0102−0853		0	0.8945	20.45 ± 0.10	—	—	18
J0106+0105		0	1.3020	20.85 ± 0.20	1.3002	20.95 ± 0.07	1
J0122−2843	B0120−28	1	0.1856	20.55 ± 0.10	0.1856	20.50 ± 0.10	4
J0126−0105		0	1.1930	20.65 ± 0.10	1.1916	20.60 ± 0.04	1
J0139−0023		0	0.6840	20.60 ± 0.15	0.6828	20.60 ± 0.07	1
J0153+0052		0	1.0610	20.35 ± 0.20	1.0599	20.43 ± 0.10	1
J0304−2212	B0302−2223	0	1.0094	20.30 ± 0.10	1.0140	20.00	5,6
J0452−1640		0	1.0090	21.00 ± 0.10	1.0072	20.98 ± 0.06	1
J0456+0400	B0454+0356	0	0.8586	20.60 ± 0.10	0.8596	20.75 ± 0.02	7
J0741+3111		0	0.2220	20.60 ± 0.20	0.2213	20.90 ± 0.07	1
J0830+2410	B0827+2421	0	0.5191	20.40 ± 0.20	0.5247	20.30 ± 0.05	1
J0930+2848	SDSS-J093001.90+284858.4	2	0.0227	20.75 ± 0.10	0.0227	20.71 ± 0.15	17
J0938+4128	B0935+4141	1	1.3725	20.45 ± 0.15	1.3960	20.50	15
J0948+4323		0	1.2340	21.75 ± 0.15	—	—	18
J0953−0038		0	0.6390	20.30 ± 0.10	0.6381	19.90 ± 0.08	1
J0954+1743		0	0.2410	21.05 ± 0.20	0.2377	21.32 ± 0.05	1
J1001+5553	B0957+5608a	0	1.3913	20.30 ± 0.20	1.3911	20.28 ± 0.08	8
J1009+0713	SDSSJ100902.06+071343.8	2	0.1139	20.75 ± 0.10	0.1140	20.68 ± 0.10	9
J1009+0036		0	0.9730	20.30 ± 0.15	0.9714	20.00 ± 0.10	1
J1010+0003		0	1.2670	21.70 ± 0.10	1.2651	21.52 ± 0.06	1
J1017+5356		0	1.3070	20.70 ± 0.10	—	—	18
J1106−1821	B1104−1805b	0	1.6617	20.80 ± 0.10	1.6616	20.84	10
J1107+0048		0	0.7410	21.00 ± 0.15	0.7470	21.00 ± 0.04	1
J1124−1705	B1122−1648	1	0.6812	20.35 ± 0.15	0.6819	20.45 ± 0.15	11
J1130−1449	B1127−1432	0	0.3140	21.30 ± 0.15	0.3130	21.71 ± 0.07	1
J1224+0037		0	1.2350	20.75 ± 0.15	1.2346	20.88 ± 0.05	1
J1225+0035		0	0.7730	21.55 ± 0.10	0.7730	21.38 ± 0.12	1
J1232−0224	Q1232−022	0	0.3950	20.85 ± 0.15	0.3950	20.75 ± 0.07	12
J1251+4637	Q1251+463	0	0.3965	20.60 ± 0.15	0.3965	20.50 ± 0.20	17
J1331+3030	B1328+3045	0	0.6840	21.40 ± 0.15	0.6920	21.30	13
J1420−0054		0	1.3470	20.85 ± 0.15	1.3475	20.90 ± 0.05	1
J1431+3952		0	0.6040	21.30 ± 0.15	0.6019	21.20 ± 0.10	16
J1501+0019		0	1.4840	20.90 ± 0.10	1.4832	20.85 ± 0.14	1
J1512+0128	SDSS-J151237.05+012846.	2	0.0295	20.40 ± 0.10	0.0295	20.27 ± 0.15	17
J1527+2452		0	0.7345	20.40 ± 0.15	—	—	18
J1537+0021		0	1.1790	20.30 ± 0.10	1.1782	20.18 ± 0.10	1
J1616+4154	SDSSJ161649.42+415416.3	2	0.3210	20.65 ± 0.20	0.3211	20.60 ± 0.20	9
J1619+3342	SDSSJ161916.54+334238.4	2	0.0964	20.65 ± 0.10	0.0963	20.55 ± 0.10	9
J1624+2345	B1622+2352	0	0.6556	20.30 ± 0.10	0.6560	20.30	14
J1712+5559		0	1.2100	20.65 ± 0.15	1.2093	20.72 ± 0.05	1
J1727+5302		0	0.9480	21.25 ± 0.15	0.9448	21.16 ± 0.05	1
J1727+5302		0	1.0330	21.50 ± 0.15	1.0312	21.41 ± 0.03	1
J1733+5533		0	0.9990	20.80 ± 0.10	0.9981	20.70 ± 0.03	1
J2334+0052		0	0.4740	20.50 ± 0.15	0.4713	20.65 ± 0.15	1
J2339−0029		0	0.9680	20.60 ± 0.15	0.9664	20.48 ± 0.08	1
J2353−0028		0	0.6044	21.50 ± 0.10	0.6044	21.54 ± 0.15	1

References. — (1) Rao et al. (2006); (2) Aracil et al. (2002); (3) Lacy et al. (2003); (4) Oliveira et al. (2014); (5) Lanzetta et al. (1995); (6) Pettini & Bowen (1997); (7) Steidel et al. (1995); (8) Zuo et al. (1997); (9) Meiring et al. (2011); (10) Lopez et al. (1999); (11) De la Varga et al. (2000); (12) Boissé et al. (1998); (13) Cohen et al. (1994); (14) Steidel et al. (1997); (15) Jannuzi et al. (1998); (16) Ellison et al. (2012); (17) Muzahid et al. (2015); (18) This Work.

[a] DLA is found in the sightline of a quasar that is: (0) not in the statistical sample; (1) in the statistical sample; (2) in the galaxy sample (see Table 1 and Section 2.1).

4. RESULTS

4.1. *The full sample of DLAs*

Figure 3 shows the H I absorption profiles for all the absorbers with a measured H I column density greater than $10^{20.3}$ cm^{-2}. These absorbers are also listed in Table 3. Our sample contains a total of 47 DLAs with a mean redshift of $z = 0.796$. Of these 47 systems, 33 were selected due to the presence of strong Mg II absorption, 6 due the presence of a galaxy close to the quasar sightline, 2 were known H I 21 cm absorbers, and 2 were known DLAs. Only 4 DLAs were discovered in sightlines not *a priori* selected to contain a strong absorber, and hence form the statistical sample of this paper.

We can test our methodology and recovery rate of DLAs by comparing our list of DLAs to those found in Rao et al. (2006), as the latter is a subset of this larger sample. We find that our search algorithm recovers 28 of the 41 DLAs in the Rao et al. (2006) sample, with a mean dispersion of 0.10 dex between the H I column density estimates. Four of the DLAs were not covered by our spectra either due to the cut-off at 1350 Å in the FOS G160L or some other reduction issue. One of these is the serendipitously discovered DLA at z=0.0912 towards B0738+313. However, we note that the omission

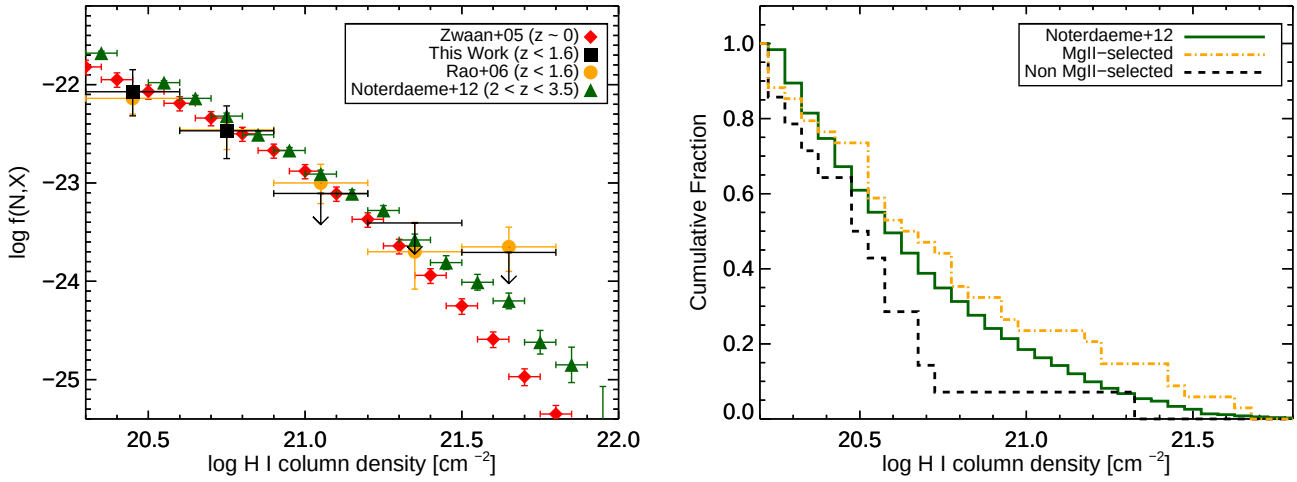

Figure 4. The H I column density distribution function, $f(N_{\rm HI}, X)$, at low redshifts. The black squares are from the present survey, and described in the text. Our results for $f(N_{\rm HI}, X)$ are consistent with earlier $f(N_{\rm HI}, X)$ estimates at both low and high redshifts (Zwaan et al. 2005; Noterdaeme et al. 2012). The high value of $f(N_{\rm HI}, X)$ found by Rao et al. (2006) at high column densities may be due to a selection effect, which would skew the distribution of $f(N_{\rm HI}, X)$ towards higher H I column density. The right panel shows that the cumulative distribution of the Mg II-selected DLAs is indeed skewed toward higher H I column densities (compared to that of the non-Mg II-selected DLAs), indicating that this is a plausible selection effect. However, we emphasize that the sample is not large enough to statistically confirm this source of bias.

of these DLAs do not affect the results in this paper, as these sightlines would not have been part of the statistical sample because of their pre-selection of Mg II absorption.

Of the remaining 9 DLAs not recovered by our search algorithm, 8 fell in a portion of the spectrum with an S/N below our criterion (see Section 3.2). We note that these sightlines are also not included in our statistical search path and therefore do not affect the conclusions presented in this paper. The only DLA (in QSO J0153+0052 at $z_{abs} = 1.0599$) which did fall in the search algorithm's search path and was not detected was not found because the trough of this potential DLA showed significant flux.

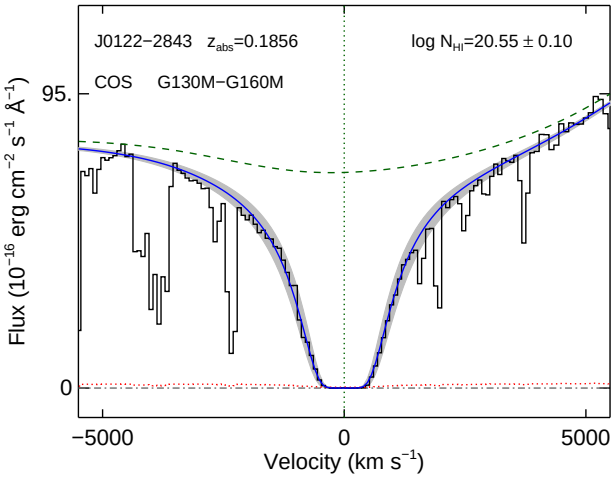

Figure 3. Example of the determination of the H I column density of an absorber. We simultaneously fit the continuum (dashed green) and the Voigt profile of the absorber to determine the H I column density. The gray shaded regions mark the error on the fit (solid blue). The dotted red line marks the uncertainty of the data. The full set of figures for all DLAs listed in Table 3 is available at the end of this manuscript or as an online figure set.

This could be either due to Ly-α emission at the redshift of the DLA, or an issue with the zero point flux of the spectrum. We have visually checked all of the spectra and believe that this is a very rare occurrence.

4.2. *The Column Density Distribution Function, $f(N_{\rm HI}, X)$*

We obtain the H I column density distribution function with the approach described in, e.g., Tytler (1987). $f(N_{\rm HI}, X)\ dN_{\rm HI}\ dX$ is defined as the number of DLAs with H I column density between $N_{\rm HI}$ and $N_{\rm HII} + dN_{\rm HI}$ and within the absorption distance dX. dX is defined as:

$$dX \equiv \frac{H_0}{H(z)}(1+z)^2 dz, \quad (1)$$

where H_0 is the Hubble constant and $H(z)$ is given by:

$$H(z) = H_0[(1+z)^2(1+z\Omega_m) - z(z+2)\Omega_\Lambda]^{-1/2}. \quad (2)$$

The absorption distance is defined in this manner such that $f(N_{\rm HI}, X)$ is constant for a non-evolving population of absorbers.

The statistical sample only contains 4 DLAs, and therefore we have poor constraints on the functional form of $f(N_{\rm HI}, X)$. To increase the sample size, we include all sightlines selected to probe an intervening galaxy (i.e. those with $f_{\rm stat} = 2$ in Table 1), resulting in a DLA sample of 9 DLAs. We note that the inclusion of these sight lines will likely bias the normalization of $f(N_{\rm HI}, X)$ high. The resulting $f(N_{\rm HI}, X)$ is shown in the left panel of Figure 4. Our results are consistent with the results of the local H I 21 cm study of Zwaan et al. (2005), and with those of DLA surveys at higher redshifts (e.g., Prochaska & Wolfe 2009; Noterdaeme et al. 2012). However, our sample size remains too small to constrain $f(N_{\rm HI}, X)$ at the highest H I column densities.

We also consider $f(N_{\rm HI}, X)$ for the sample described in Rao et al. (2006). They note that their sample con-

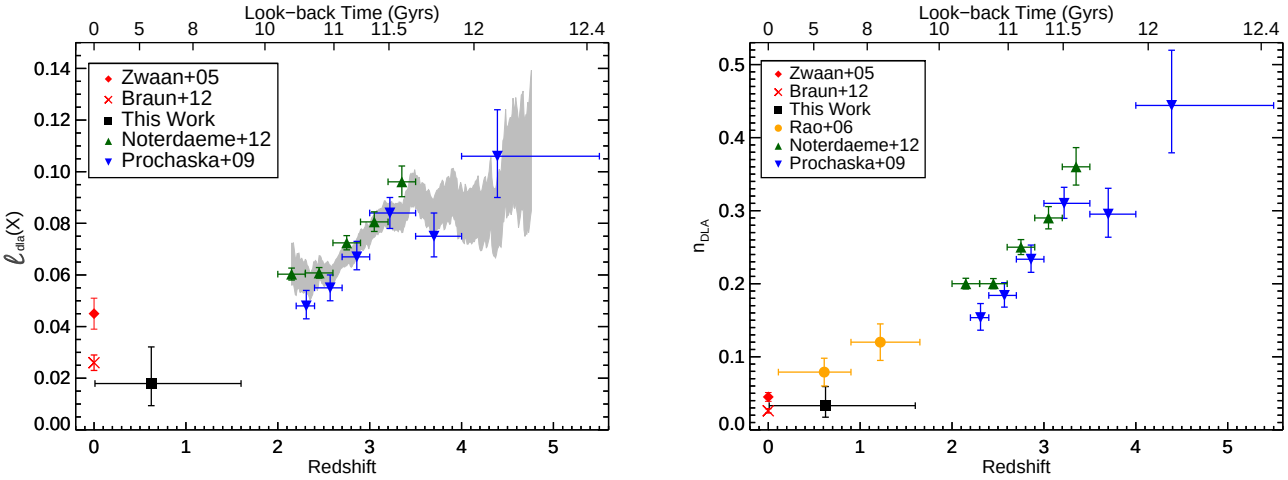

Figure 5. *Left panel:* Line density of DLAs, $\ell_{\rm DLA}(X)$ and *Right panel:* Redshift number density of DLAs, $n_{\rm DLA}$. The gray area marks the 68 % confidence level for the sample compiled by Sánchez-Ramírez et al. (2015). The line density of DLAs over the redshift interval $z \approx 0.01$ to $z \approx 1.6$ is lower than the measured line density at redshift $z \approx 2$ at greater than 2-σ significance, indicating that $\ell_{\rm DLA}(X)$ has evolved over the past 10 Gyrs.

tains a large number of high H I column density systems, although this deviation is not statistically significant. We have broken up our sample into those DLAs that were found using the Mg II selection criteria defined in Rao et al. (2006) and the remaining DLAs. The cumulative distribution plotted in the right panel of Figure 4 indeed shows that the Mg II-selected DLA sample has a larger number of high H I column density systems than the rest of the low-z DLA sample (this work) or the high-z DLA sample of Noterdaeme et al. (2012). This corroborates the suggestion of Prochaska & Wolfe (2009) that selecting sightlines based on metal line absorption could bias the H I distribution toward high column densities. This result is also seen in recent work on metal-strong absorbers (Dessauges-Zavadsky et al. 2009; Kaplan et al. 2010; Berg et al. 2015).

4.3. *Line density of DLAs, $\ell_{\rm DLA}(X)$*

The line density of DLAs, $\ell_{\rm DLA}(X)$, is defined as the zeroth moment of $f(N_{\rm HI}, X)$, i.e.:

$$\ell_{\rm DLA}(X) = \int_{N_{\rm DLA}}^{\infty} f(N_{\rm H\,I}, X) dN dX, \qquad (3)$$

where $N_{\rm DLA}$ is the threshold H I column density for DLAs. In practice, $\ell_{\rm DLA}(X)$ is estimated by measuring the number of DLAs in a given redshift bin and then dividing this value by the total absorption path length in this redshift bin. A correlated quantity is the redshift number density, $n_{\rm DLA}$, which is obtained by dividing the number of DLAs found in a redshift bin by the redshift path length. Both of these quantities describe the incidence rate of DLAs along a line of sight.

We have calculated $\ell_{\rm DLA}(X)$ and $n_{\rm DLA}$ for the complete statistical sample (those with $\rm f_{stat} = 1$), which covers the redshift range, $z = 0.01 - 1.6$, with a median redshift of 0.623. The resultant $\ell_{\rm DLA}(X)$ is $0.017^{+0.014}_{-0.008}$, which equates to $n_{\rm DLA} = 0.033^{+0.026}_{-0.015}$. These values are put in context by plotting them with a compilation from the literature in Figure 5.

Figure 5 shows that the line density obtained from this sample is lower than the locally measured values of Zwaan et al. (2005) and Braun (2012) (note that the latter estimate is based on an extrapolation from just three galaxies), although our estimate is consistent with these values within 2-σ significance. Our $\ell_{\rm DLA}(X)$ estimate is also lower than the estimate of Rao et al. (2006), but the systematic uncertainties in their measurement are difficult to quantify.

Our new estimate of the line density of DLAs at $z < 1.6$ is lower than this value at $z \sim 2$ (Noterdaeme et al. 2012) at greater than 2-σ significance. This result suggests that $\ell_{\rm DLA}(X)$ has evolved over this redshift range. This result is discussed further in Section 5.

We note that we have searched for evolution within our sample by dividing the sample into two subsamples at the median redshift of $z = 0.623$. However, the sample size is too small to discern any evolution within the sample, although the sample is consistent with an evolution of < 0.05 in $\ell_{\rm DLA}(X)$ per unit redshift, which agrees with the evolution at higher redshift (~ 0.03 in $\ell_{\rm DLA}(X)$ per unit redshift, see e.g., Sánchez-Ramírez et al. (2015)).

4.4. *Mass Density of H I, $\rho_{\rm HI}^{\rm DLA}$*

The final quantity we consider is the first moment of $f(N_{\rm HI}, X)$, which is the mass density of H I contained in DLAs, $\rho_{\rm HI}^{\rm DLA}$. This quantity is defined by:

$$\rho_{\rm H\,I}^{\rm DLA} = \frac{m_{\rm H} H_0}{c} \int_{N_{\rm min}}^{N_{\rm max}} N_{\rm H\,I} f(N_{\rm H\,I}, X) dN dX, \qquad (4)$$

where $m_{\rm H}$ is the mass of the hydrogen atom and c is the speed of light. The superscript clarifies that we are only measuring the fraction of H I in DLAs; of course, as noted earlier, these systems contain the bulk (> 85 %) of the H I at all redshifts (Zwaan et al. 2005; O'Meara et al. 2007; Noterdaeme et al. 2012). We also note that literature studies often provide estimates of the cosmological neutral gas mass density, $\Omega_g^{\rm DLA}$. $\rho_{\rm HI}^{\rm DLA}$ is related to $\Omega_g^{\rm DLA}$ by the conversion factor μ/ρ_c, where μ is the mean molecular mass of the gas and ρ_c is the critical density of the Universe.

As with $f(N_{\rm HI}, X)$, $\rho_{\rm HI}^{\rm DLA}$ cannot be accurately determined from our own study because the small sample size

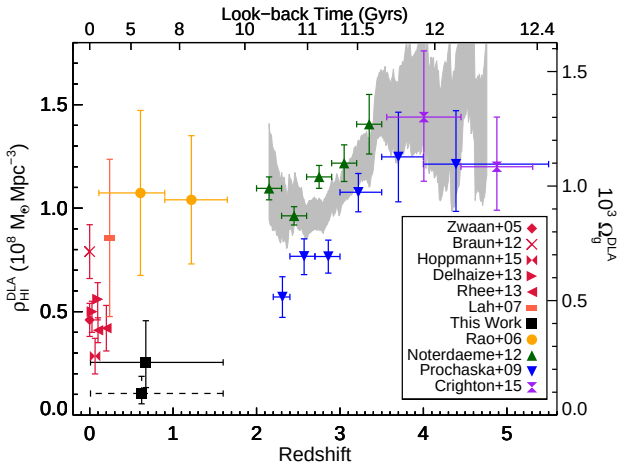

Figure 6. Mass density of H I in DLAs, $\rho_{\rm HI}^{\rm DLA}$. The dashed point is the unadjusted measurement not accounting for the small sample size, whereas the solid black point accounts for the sample size (see text). The gray area, as in Figure 5a, marks the 68 % confidence level of $\rho_{\rm HI}^{\rm DLA}$ for the sample compiled by Sánchez-Ramírez et al. (2015). The literature estimates of $\Omega_{\rm H\,I}$ were converted to $\rho_{\rm HI}^{\rm DLA}$ by assuming 85 % of the cosmic H I is in DLA gas. The data indicates a slow decrease in $\rho_{\rm HI}^{\rm DLA}$ over the past 10 Gyrs.

lacks the statistics to accurately determine the number of high H I column density ($N_{\rm HI} \gtrsim 10^{21}$ cm^{-2}) systems (none are present in our survey). These systems are likely to contribute significantly to $\rho_{\rm HI}^{\rm DLA}$ (Zwaan et al. 2005; O'Meara et al. 2007; Noterdaeme et al. 2012), and our results are hence likely to underestimate the underlying neutral gas density. To account for this, we assume that the mean column density of the low redshift absorber sample is unchanged from the mean column density at high redshifts, as measured by Noterdaeme et al. (2012) (see Section 4.2).

Our data yield $\rho_{\rm HI}^{\rm DLA}$=$(0.10^{+0.08}_{-0.05} \times 10^8 M_\odot {\rm Mpc}^{-3})$ over the redshift range $0.01 \lesssim z \lesssim 1.6$, without any correction for the missing high H I column density absorbers. Using the mean H I column density estimate of Noterdaeme et al. (2012) to account for their absence, we obtain a corrected $\rho_{\rm HI}^{\rm DLA}$ of $0.25^{+0.20}_{-0.12} \times 10^8 M_\odot {\rm Mpc}^{-3}$. Both the corrected (solid error bars) and uncorrected (dashed error bars) values are shown in Figure 6, along with other estimates of this quantity at different redshifts from the literature.

Our corrected estimate of $\rho_{\rm HI}^{\rm DLA}$ is lower than the earlier estimate over the same redshift range by Rao et al. (2006). The lower value compared to that of Rao et al. (2006) is due to both the decrease in $\ell_{\rm DLA}(X)$ and the lower adopted mean H I column density (see Section 4.2). Our H I mass density estimate is, however, in good agreement with the estimates from H I 21 cm studies at $z \approx 0-0.3$ (Zwaan et al. 2005; Lah et al. 2007; Delhaize et al. 2013; Rhee et al. 2013; Hoppmann et al. 2015). The results suggest a mild evolution in $\rho_{\rm HI}^{\rm DLA}$, driven by the evolution in $\ell_{\rm DLA}(X)$, which was recently quantified by Crighton et al. (2015) and Sánchez-Ramírez et al. (2015) who measured $\rho_{\rm HI}^{\rm DLA}$ at high redshifts.

Finally, we would like to point out the apparent discrepancy in the $\rho_{\rm HI}^{\rm DLA}$ measurements of Prochaska & Wolfe (2009) and Noterdaeme et al. (2012) at $z \approx 3$. This discrepancy is due to two factors: (i) the sample analyzed by Prochaska & Wolfe (2009) led to an under-estimate in the break in $f(N_{\rm HI}, X)$ by $\approx$ 0.2 dex and therefore an under-estimate of $\rho_{\rm HI}$ by $\approx$ 20 %; (ii) the results are now limited by systematic uncertainties that include the approach to measuring $N_{\rm HI}$, dust obscuration, and color-selection bias in quasar surveys. These systematic errors must be addressed before further progress can be made in this field.

5. SUMMARY AND DISCUSSION

In this paper, we have used a large sample of quasars (767 systems) observed with the UV spectrographs on the Hubble Space Telescope to carry out a search for low-redshift DLAs. Of the 46 DLAs found in this study, only 4 are drawn from the statistical sample. The remainder were drawn from sightlines with foreknowledge of either an absorber or an intervening galaxy, or the lack of an absorber, close to or along the quasar line of sight.

Our statistical sample enables an unbiased determination of the line density of DLAs, $\ell_{\rm DLA}(X)$, over the redshift range $0.01 \lesssim z \lesssim 1.6$. We obtain $\ell_{\rm DLA}(X) = 0.017^{+0.014}_{-0.008}$, significantly smaller than the previous estimate of Rao et al. (2006), which appears likely to be biased high. Unfortunately, current estimates of $\ell_{\rm DLA}(X)$ at these redshifts continue to suffer from the small sample size of quasar sightlines.

Previous studies, e.g., Prochaska et al. (2005); Rao et al. (2006); Prochaska & Wolfe (2009); Noterdaeme et al. (2012), have claimed little evolution in the line density of DLAs in the past 10 Gyrs. However, the results in this paper indicate that the line density at $z \approx 0.5$ is lower than estimates of this quantity at $z \approx 2$ at greater than 2-σ significance. This suggests a mild evolution in $\ell_{\rm DLA}(X)$ from $z \approx 2$ to the present epoch, instead of the inferred constancy in the DLA line density. The decrease in $\ell_{\rm DLA}(X)$ at low redshifts can be explained if the majority of galactic-scale dark matter halos are fully assembled by $z \approx 2$, and, if the neutral hydrogen content of these halos slowly decreases, either by star formation or feedback processes.

One caveat to this result is the possibility of systematic errors that can bias our estimates low. Here we discuss three of these biases. One potential bias to our sample is the exclusion of sightlines that were targeted to pass close to foreground galaxies. A random sample of quasars would contain some sightlines that pass by intervening galaxies, and by removing all of these quasars from the sample, we could be biasing our result low. To estimate the effect of this potential bias, we include all sightlines that are specifically chosen to cross a foreground galaxy (i.e. the quasars with $f_{\rm stat} = 2$). The resultant line density is $\ell_{\rm DLA}(X) = 0.030^{+0.014}_{-0.010}$, which is well within the 1-σ statistical uncertainty of our original estimate, indicating that this bias is smaller than our uncertainties.

A second possible bias may arise due to the inclusion of sightlines at redshifts $z \gtrsim 0.3$. For these redshifts, metal lines (in particular Mg II) would fall within the optical part of the quasar spectrum. The target selection criteria for the quasar sample may have included a lack of metal line systems in the optical part of the quasar spectrum. Similarly, by excluding all of the sightlines with known Mg II systems, we might be biasing ourselves against quasars with metal lines in their sightlines. To test the

bias in our sample against Mg II systems, we have compared the line density of Mg II systems in our quasar sample with the line density in the sample of Seyffert et al. (2013). We find that the line density of Mg II systems is 0.119 over the full redshift range probed by the quasars in our statistical sample, which are also part of the sample of Seyffert et al. (2013) (n=93 quasars). This value agrees well with the measured line density of 0.123±0.001 over the slightly larger redshift range covered by the full sample of Seyffert et al. (2013), and hence we assert that this effect is unlikely to significantly bias our results.

Finally, the third possible source of bias is that against sightlines with a large amount of dust. This bias has been studied in detail using spectroscopy of radio-selected samples in high-z DLAs (e.g., Ellison et al. 2001; Akerman et al. 2005; Jorgenson et al. 2006) as well as dust reddening of quasars in SDSS (e.g., Murphy & Liske 2004; Frank et al. 2010; Fukugita & Ménard 2015; Murphy & Bernet 2016). This bias is correlated with the amount of metals in the gas (Vladilo & Péroux 2005), and therefore is amplified at low-z due to the higher metallicity of low-z DLAs (e.g., Prochaska et al. 2003; Rafelski et al. 2012, 2014).

Following Vladilo & Péroux (2005), dust extinction becomes significant at zinc column densities greater than $\sim 10^{13.5}\,\mathrm{cm}^{-2}$, an assertion corroborated by the few DLAs showing distinct dust signatures (Noterdaeme et al. 2009a; Kulkarni et al. 2011; Ma et al. 2015). For low column density DLAs ($\log N_{\rm HI} < 20.5$) these zinc column densities imply $[M/H] > 0.5$. Such systems are expected to be rare, both from metallicity measurements of lower column density systems, and metallicity measurements from star-forming galaxies (e.g. Tremonti et al. 2004). Since $\ell_{\rm DLA}(X)$ is dominated by low H I column density systems, we assert that the effect of dust on biasing this result is small. In passing, we note that the amount of dust reddening in quasars with DLAs is observed to be small at $z \approx 2$ (Murphy & Liske 2004), and evolves only slightly between redshifts 2.1 and 4.0 (Murphy & Bernet 2016) further suggesting that dust is not likely a large biasing factor.

We estimate the H I column density distribution function, $f(N_{\rm HI}, X)$, and the H I gas density, $\rho_{\rm HI}^{\rm DLA}$ from our statistical sample. However, the limited sample size means that the errors on the inferred quantities are large. We find that the H I column density distribution function in our low redshift sample is consistent with the $f(N_{\rm HI}, X)$ measured at high redshift. The increase in the high H I column density systems found by Rao et al. (2006) could be due to their selection process, but we cannot establish this assertion with the current dataset.

The H I mass density, $\rho_{\rm HI}^{\rm DLA}$, is estimated to be $0.25^{+0.20}_{-0.12} \times 10^8 M_\odot \mathrm{Mpc}^{-3}$, after correcting for the lack of statistics at the high H I column density end due to our small sample size of DLAs. The correction makes the assumption that the mean H I column density of our low-z DLA sample is the same as that of the high-z DLA sample, as measured from the SDSS surveys (Noterdaeme et al. 2012). Our value of $\rho_{\rm HI}^{\rm DLA}$ is markedly lower than that obtained in previous measurements at these redshifts, but is in agreement with estimates of the H I mass density at $z \lesssim 0.3$ using H I 21 cm studies (Zwaan et al. 2005; Lah et al. 2007; Delhaize et al. 2013; Rhee et al. 2013; Hoppmann et al. 2015). The apparent mild evolution seen in $\rho_{\rm HI}^{\rm DLA}$ from $z \approx 2$ arises due to the evolution in $\ell_{\rm DLA}(X)$, since we have assumed a non-evolving mean H I column density.

In conclusion, this study has compiled the largest sample of quasars observed in the UV with spectral resolution sufficient to search for low-redshift DLAs. Even with a total of 767 quasars in our target sample, the final sample of DLAs in these spectra is small, containing only 46 DLAs. This is in part due to the smaller than expected incidence rate of DLAs compared to the measurements from Mg II surveys (Rao et al. 2006). However, the lower incidence rate is in agreement with both the results at $z \approx 2$ and $z \approx 0$, if we assume a mild decrease in $\ell_{\rm DLA}(X)$ over this redshift range.

This research would not have been possible without the guidance and insights of the late A. M. Wolfe during the initial phases of the project. He will be sorely missed. We thank R. Sánchez-Ramírez for providing their results before publication, and the referee for helpful comments that improved the manuscript. This work was based on observations made with the NASA/ESA Hubble Space Telescope, obtained from the data archive at the Space Telescope Science Institute (STScI). The COS G130M/G160M data presented in this work were obtained from the COS-CGM Legacy database, which is funded by NASA through grant HST-AR-12854 from the STScI. Finally, support for this work was provided by NASA through grant HST-AR-12645 from the STScI. STScI is operated by the Association of Universities for Research in Astronomy, Inc. under NASA contract NAS 5-26555. MN and JXP further acknowledge support from NSF award AST-1109452. NL acknowledges support provided by NASA through grant HST-AR-12854. JCH and NL acknowledge support from NSF award AST-1212012. MR acknowledges support from an appointment to the NASA Postdoctoral Program at Goddard Space Flight Center. NK acknowledges support from the Department of Science and Technology via a Swarnajayanti Fellowship (DST/SJF/PSA-01/2012-13).

REFERENCES

Abazajian, K. N., Adelman-McCarthy, J. K., Agüeros, M. A., et al. 2009, ApJS, 182, 543
Akerman, C., Ellison, S. L., Pettini, M., & Steidel, C. C. 2005, A&A, 440, 499
Aracil, B., Petitjean, P., Smette, A., et al. 2002, A&A, 391, 1
Bechtold, J., Dobrzycki, A., Wilden, B., et al. 2002, ApJS, 140, 143
Berg, T. A., Neeleman, M., Prochaska, J. X., Ellison, S. L., & Wolfe, A. M. 2015, PSAP, 127, 167
Boissé, P., Le Brun, V., Bergeron, J., & Deharveng, J.-M. 1998, A&A, 333, 841
Braun, R. 2012, ApJ, 749, 87
Briggs, F. H., & Wolfe, A. M. 1983, ApJ, 268, 76
Catinella, B., & Cortese, L. 2015, MNRAS, 446, 3526
Catinella, B., Haynes, M. P., Giovanelli, R., Gardner, J. P., & Connolly, A. J. 2008, ApJ, 685, L13
Cohen, R. D., Barlow, T., Beaver, E., et al. 1994, ApJ, 421, 453
Crighton, N., Murphy, M., Prochaska, J. X., et al. 2015, MNRAS, 452, 217
De la Varga, A., Reimers, D., Tytler, D., Barlow, T., & Burles, S. 2000, A&A, 363, 69
Delhaize, J., Meyer, M., Staveley-Smith, L., & Boyle, B. 2013, MNRAS, 433, 1398

Dessauges-Zavadsky, M., Ellison, S. L., & Murphy, M. T. 2009, MNRAS, 396, L61
Ellison, S. L., Kanekar, N., Prochaska, J. X., Momjian, E., & Worseck, G. 2012, MNRAS, 424, 293
Ellison, S. L., Yan, L., Hook, M., et al. 2001, A&A, 379, 393
Fernández, X., van Gorkom, J. H., Hess, K. M., et al. 2013, ApJL, 770, L29
Frank, S., Mathur, S., Pieri, M., & York, D. 2010, AJ, 140, 835
Fukugita, M., & Ménard, B. 2015, ApJ, 799, 195
Hoppmann, L., Staveley-Smith, L., Freudling, W., et al. 2015, MNRAS, 452, 3726
Jannuzi, B. T., Bahcall, J. N., Bergeron, J., et al. 1998, ApJS, 118, 1
Jorgenson, R., Wolfe, A. M., Prochaska, J. X., et al. 2006, ApJ, 646, 730
Kanekar, N., Prochaska, J. X., Ellison, S. L., & Chengalur, J. N. 2009, MNRAS, 396, 385
Kaplan, K. F., Prochaska, J. X., Herbert-Fort, S., Ellison, S. L., & Dessauges-Zavadsky, M. 2010, PSAP, 122, 619
Kulkarni, V., Torres-Garcia, L., Som, D., et al. 2011, ApJ, 726, 14
Lacy, M., Becker, R., Storrie-Lombardi, L., et al. 2003, AJ, 126, 2230
Lah, P., Chengalur, J. N., Briggs, F. H., et al. 2007, MNRAS, 376, 1357
Lanzetta, K. M., Wolfe, A. M., & Turnshek, D. A. 1995, ApJ, 440, 435
Lanzetta, K. M., Wolfe, A. M., Turnshek, D. A., et al. 1991, ApJ, 77, 1
Lopez, S., Reimers, D., Rauch, M., Sargent, W. L., & Smette, A. 1999, ApJ, 513, 598
Ma, J., Caucal, P., Noterdaeme, P., et al. 2015, MNRAS, 451, 1751
Meiring, J., Tripp, T., Prochaska, J. X., et al. 2011, ApJ, 732, 35
Murphy, M., & Bernet, M. 2016, MNRAS, 455, 1043
Murphy, M., & Liske, J. 2004, MNRAS, 354, 31
Muzahid, S., Srianand, R., & Charlton, J. 2015, MNRAS, 448, 2840
Noterdaeme, P., Ledoux, C., Srianand, R., Petitjean, P., & Lopez, S. 2009a, A&A, 503, 765
Noterdaeme, P., Petitjean, P., Ledoux, C., & Srianand, R. 2009b, A&A, 505, 1087
Noterdaeme, P., Petitjean, P., Carithers, W., et al. 2012, A&A, 547, L1
Oliveira, C., Sembach, K., Tumlinson, J., O'Meara, J., & Thom, C. 2014, ApJ, 783, 22
O'Meara, J., Prochaska, J. X., Burles, S., et al. 2007, ApJ, 656, 666
Pettini, M., & Bowen, D. V. 1997, A&A, 327, 22
Prochaska, J. X., Gawiser, E., Wolfe, A. M., Castro, S., & Djorgovski, S. 2003, ApJ, 595, L9
Prochaska, J. X., Gawiser, E., Wolfe, A. M., Cooke, J., & Gelino, D. 2003a, ApJS, 147, 227
Prochaska, J. X., Herbert-Fort, S., & Wolfe, A. M. 2005, ApJ, 635, 123
Prochaska, J. X., & Wolfe, A. M. 2009, ApJ, 696, 1543
Rafelski, M., Neeleman, M., Fumagalli, M., Wolfe, A. M., & Prochaska, J. X. 2014, ApJ, 782, L29
Rafelski, M., Wolfe, A. M., Prochaska, J. X., Neeleman, M., & Mendez, A. 2012, ApJ, 755, 21
Rao, S. M., & Turnshek, D. A. 2000, ApJS, 130, 1
Rao, S. M., Turnshek, D. A., & Nestor, D. B. 2006, ApJ, 636, 610
Rhee, J., Zwaan, M., Briggs, F., et al. 2013, MNRAS, 435, 2693
Ribaudo, J., Lehner, N., & Howk, J. C. 2011, ApJ, 736, 42
Sánchez-Ramírez, R., Ellison, S. L., Prochaska, J. X., et al. 2015, MNRAS, submitted
Seyffert, E. N., Cooksey, K. L., Simcoe, R. A., et al. 2013, ApJ, 779, 161
Steidel, C. C., Bowen, D. V., Blades, J. C., & Dickinson, M. 1995, ApJ, 440, L45
Steidel, C. C., Dickinson, M., Meyer, D. M., Adelberger, K. L., & Sembach, K. 1997, ApJ, 480, 568
Thom, C., Werk, J., Prochaska, J. X., et al. 2011, ApJ, 736, 1
Tremonti, C., Heckman, T., Kauffmann, G., et al. 2004, ApJ, 613, 898
Tytler, D. 1987, ApJ, 321, 49
Vladilo, G., & Péroux, C. 2005, A&A, 444, 461
Wolfe, A. M., Gawiser, E., & Prochaska, J. X. 2005, ARA&A, 43, 861
Wolfe, A. M., Turnshek, D. A., Smith, H. E., & Cohen, R. D. 1986, ApJS, 61, 249
Zuo, L., Beaver, E., Burbidge, E., et al. 1997, ApJ, 477, 568
Zwaan, M., Meyer, M., Staveley-Smith, L., & Webster, R. 2005, MNRAS, 359, L30
Zwaan, M. A., van Dokkum, P. G., & Verheijen, M. A. W. 2001, Science, 293, 1800

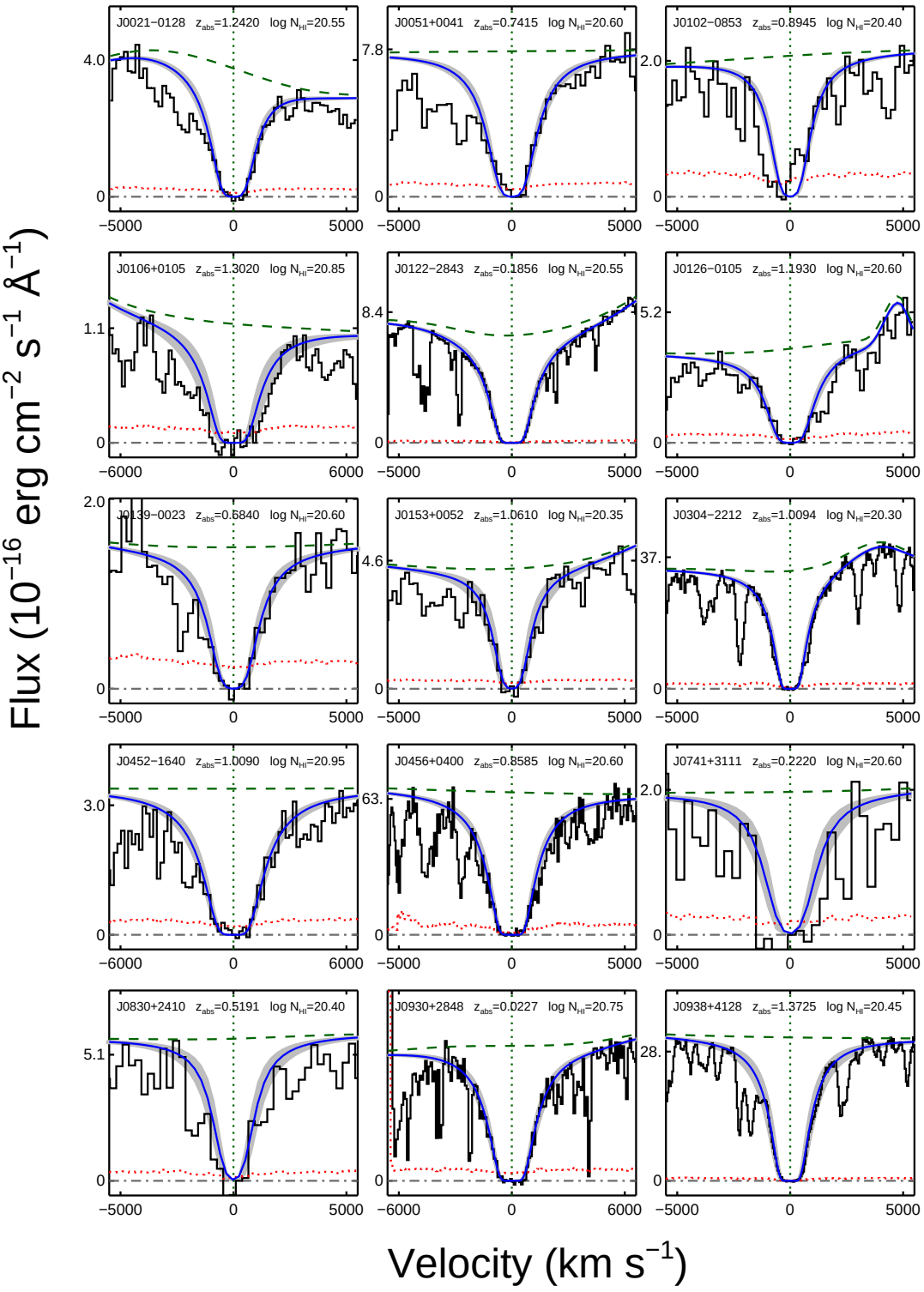

Figure 3. – Continued

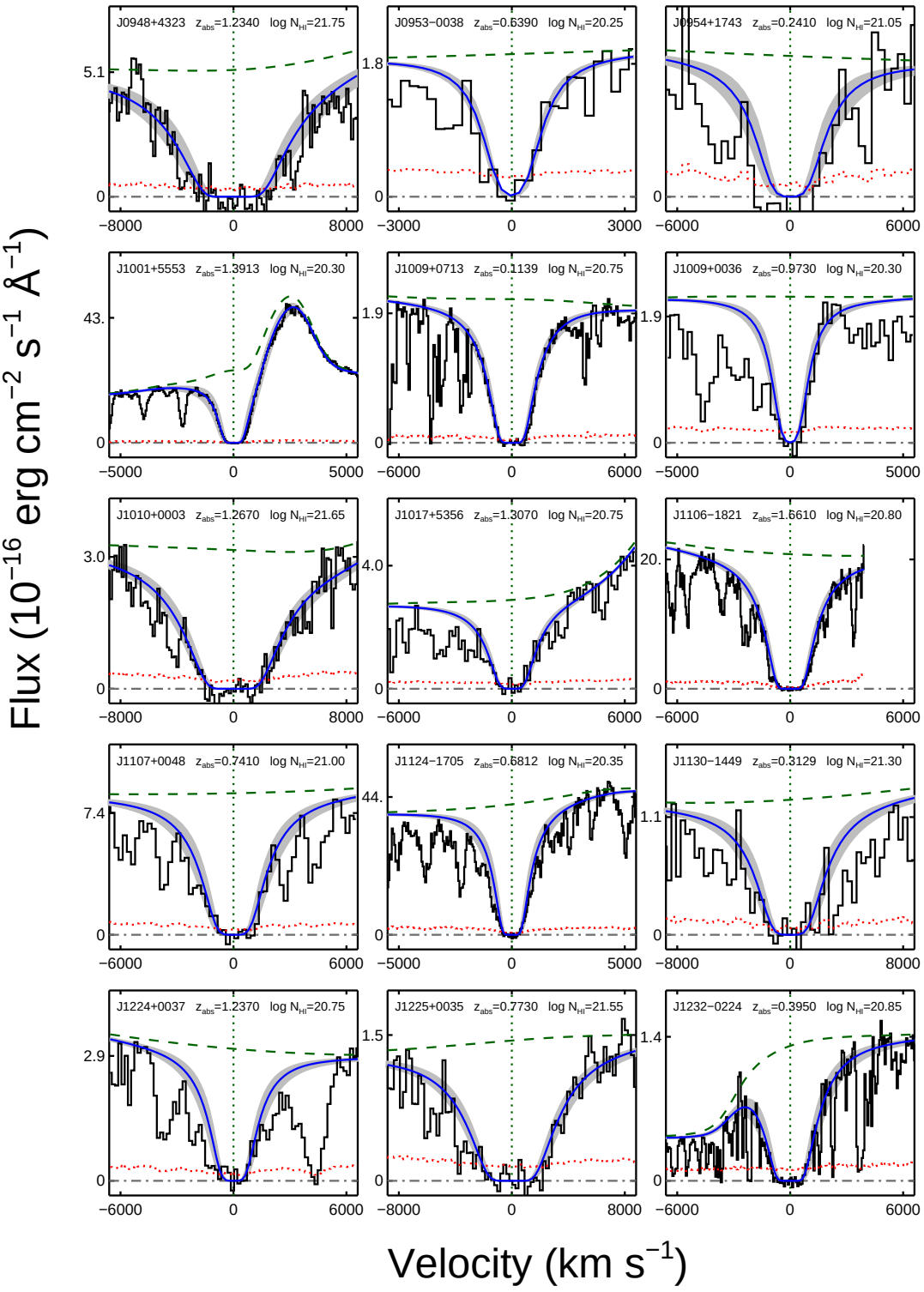

Figure 3. – Continued

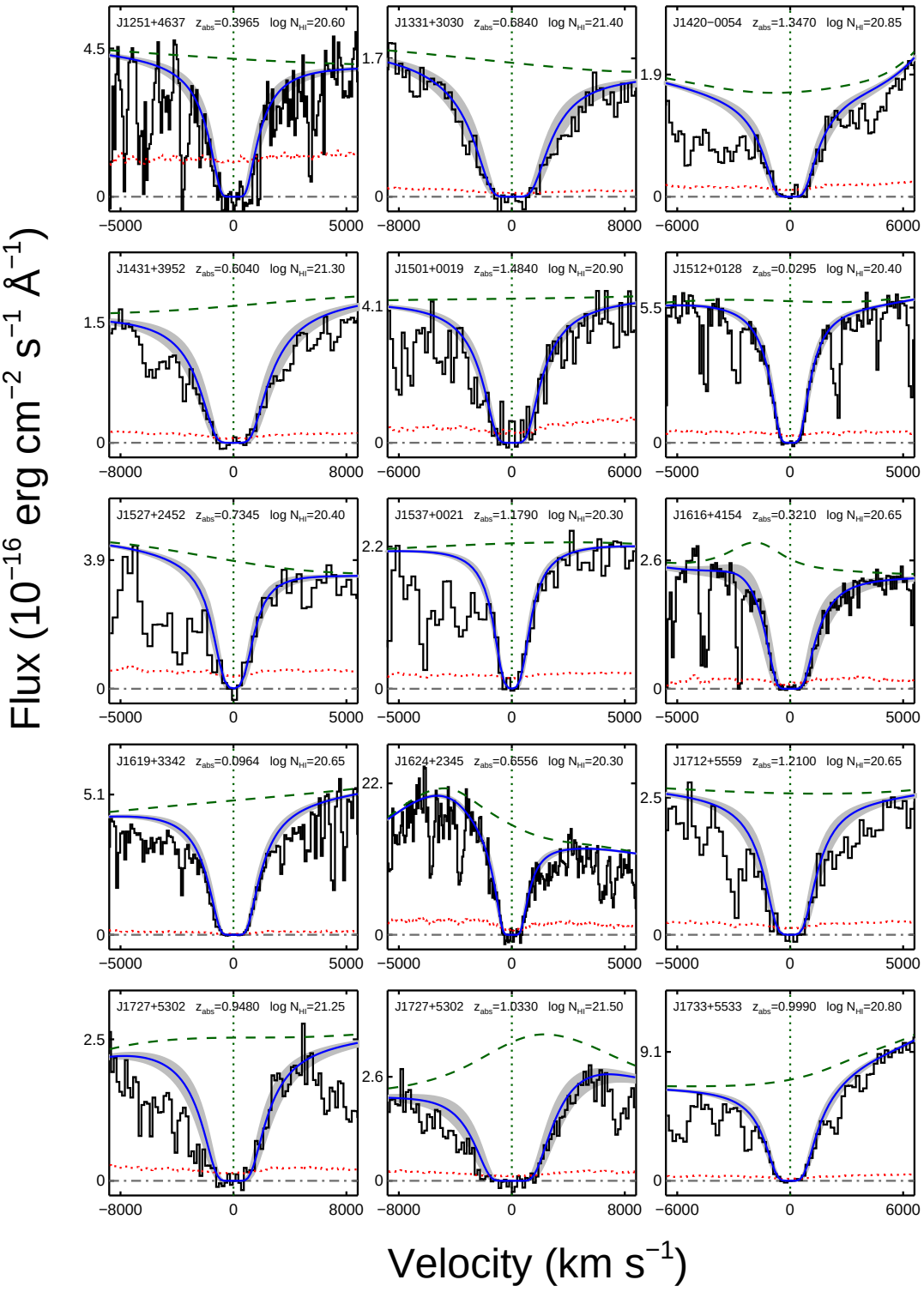

Figure 3. – Continued

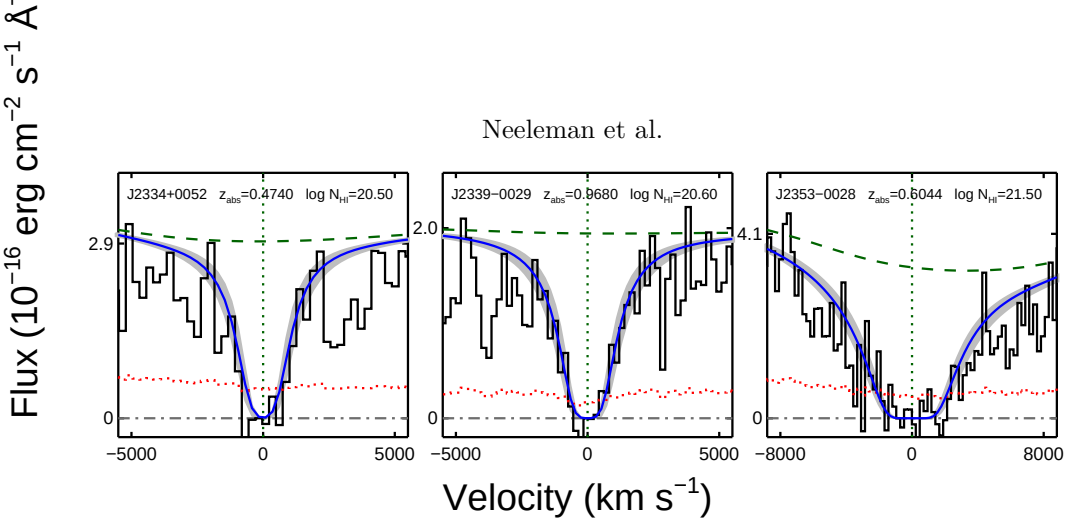

Figure 3. – Continued

Table 1
QSO sample

QSO	z_{em} [a]	Instrument	Grating	Search Path			Statistical Path			Proposal ID
				F_{search} [b]	Min z	Max z	F_{stat} [c]	Min z	Max z	
J0000−1245	0.200	COS	G130M-G160M	1	0.010	0.299	1	0.010	0.188	12604
J0001+0709	3.234	STIS	G230L	1	—	—	0	—	—	8569
J0004−4157	2.760	FOS	G270H	1	1.501	1.695	0	—	—	6577
J0005+0524	1.900	FOS	G270H-G190H	1	0.829	1.695	1	0.829	1.695	4581,6705
J0005−5006	0.033	COS	G130M-G160M	1	0.010	0.133	1	0.010	0.022	12936
J0005+0202	0.234	FOS	G190H	1	—	—	1	—	—	5456
J0005+1609	0.450	COS	G130M-G160M	1	0.010	0.474	1	0.010	0.436	12038
		FOS	G190H-G270H-G130H	1	0.475	0.550	1	—	—	3791
J0006+2012	0.025	COS	G130M-G160M	1	0.010	0.124	1	0.010	0.014	11524
		FOS	G130H-G190H-G270H	1	—	—	1	—	—	5182
J0010+1058	0.090	COS	G130M	1	0.014	0.189	1	0.014	0.079	12569
		FOS	G130H-G270H	1	—	—	2	—	—	2717
J0012−0122	1.998	STIS	G230L	1	0.862	1.604	0	—	—	8569
J0012−1022	0.228	COS	G130M-G160M	1	0.010	0.328	2	0.010	0.215	12248
J0018+1629	0.553	FOS	G190H	1	0.378	0.652	2	0.378	0.537	6606
J0018−3529	3.190	STIS	G140L	0	—	—	1	—	—	8287
J0020+0226	0.401	FOS	G190H	1	0.369	0.500	1	0.369	0.387	5456
J0020+2842	0.509	FOS	G270H	1	—	—	2	—	—	6548
J0021+0104	1.829	STIS	G230L	1	0.288	1.589	0	—	—	9382
J0021+0043	1.243	STIS	G230L	1	0.505	1.343	0	—	—	9382
J0021−0128	1.588	STIS	G230L	1	0.816	1.607	1	0.816	1.562	8126
J0022−0128	1.040	STIS	G230L	1	0.410	1.139	1	0.410	1.019	8126
J0027+2242	1.108	FOS	G270H-G190H	1	0.366	1.207	1	0.366	1.087	2424,4117
		FOS	G160L	1	—	—	1	—	—	2424
J0028+4308	0.097	COS	G130M	0	—	—	2	—	—	12533
J0029+1316	0.142	COS	G130M	1	0.010	0.192	1	0.010	0.130	12569
		FOS	G130H-G190H-G270H	1	0.193	0.241	1	—	—	5451,5682
J0032−2144	0.806	STIS	G230L	1	0.533	0.905	1	0.533	0.788	8225
J0036+4316	0.120	COS	G130M-G160M	1	0.010	0.219	2	0.010	0.108	11632
J0036−3333	0.020	COS	G130M-G160M	0	—	—	2	—	—	13017
J0038−3501	1.199	STIS	G230L	1	0.404	1.298	1	0.404	1.177	8126
J0038−3504	1.519	STIS	G230L	1	0.576	1.610	1	0.576	1.493	8126
J0039−3529	1.095	STIS	G230L	1	0.396	1.194	1	0.396	1.074	8126
J0039−3528	0.836	STIS	G230L	1	0.424	0.935	1	0.424	0.817	8126
J0040−1109	0.027	COS	G160M	0	—	—	1	—	—	12557
J0042−1037	0.423	COS	G130M-G160M	1	0.010	0.476	2	0.010	0.409	11598
J0043−2622	3.053	STIS	G230L	1	1.204	1.608	0	—	—	8569
J0044+1026	0.583	FOS	G190H-G270H	1	0.563	0.682	1	0.563	0.567	5441
J0045+0410	0.384	FOS	G190H-G270H	1	0.369	0.483	1	0.369	0.370	2424
J0047+0319	0.624	COS	G130M	1	0.010	0.206	1	0.010	0.206	12275
		FOS	G190H-G270H	1	0.362	0.723	1	0.362	0.607	2424
		FOS	G160L	1	0.360	0.361	1	0.360	0.361	2424
J0048+3941	0.134	COS	G130M-G160M	1	0.010	0.233	2	0.010	0.122	11632
J0051+0041	1.188	STIS	G230L	1	0.516	1.287	0	—	—	9051
J0053+1241	0.060	COS	G130M	1	0.010	0.160	1	0.010	0.050	12569
		FOS	G270H-G190H-G130H	1	—	—	1	—	—	5057,5486
J0054+2525	0.155	FOS	G190H	1	—	—	1	—	—	4396
J0058−3606	0.162	COS	G130M-G160M	1	0.010	0.261	1	0.010	0.150	12604
J0100−5113	0.062	COS	G130M-G160M	1	0.010	0.161	1	0.010	0.051	12604
		STIS	G140L	1	—	—	2	—	—	9858
J0100+0211	1.954	FOS	G190H	1	0.526	0.901	0	—	—	6577
J0101+4229	0.190	COS	G130M-G160M	1	0.010	0.289	2	0.010	0.178	11632
J0102−0853	1.682	STIS	G230L	1	0.777	1.598	0	—	—	9051
J0102−2221	0.118	COS	G130M	1	0.010	0.179	2	0.010	0.106	12533
J0103+0220	0.394	FOS	G190H	1	0.362	0.493	1	0.362	0.380	4396,6612
J0103−3009	3.150	STIS	G140L	0	—	—	1	—	—	8287
J0104−2657	0.780	FOS	G190H	1	0.343	0.879	1	0.343	0.762	6007
J0105−2736	0.848	STIS	G230L	1	0.527	0.947	1	0.527	0.829	7359
J0106+0105	1.611	STIS	G230L	1	0.900	1.607	0	—	—	9382
J0107−0019	0.737	STIS	G230L	1	0.363	0.837	0	—	—	9382
J0109−2307	0.818	STIS	G230L	1	0.402	0.917	1	0.402	0.799	8225
J0109−2102	0.000	STIS	G140L	0	—	—	1	—	—	8287
J0109−1521	0.861	FOS	G270H	1	0.830	0.960	2	0.830	0.842	6548
J0110−0219	0.960	COS	G130M-G160M	1	0.010	0.480	1	0.010	0.480	11585
		FOS	G190H	1	0.481	0.901	1	0.481	0.901	5320,6100,6592
J0110−0216	0.728	COS	G160M	1	0.179	0.482	1	0.179	0.482	11585
J0110−0218	0.956	COS	G130M-G160M	1	0.010	0.480	1	0.010	0.480	11585
		FOS	G190H	1	0.481	0.901	1	0.481	0.901	5320,6100
J0110+0019	0.806	STIS	G230L	2	—	—	0	—	—	9382
J0111+1753	2.157	FOS	G160L	0	—	—	1	—	—	5095
J0115−0127	1.365	FOS	G270H	1	0.879	1.464	1	0.879	1.341	2578
J0116−0043	1.273	STIS	G230L	1	0.570	1.373	0	—	—	9382
J0118+0258	0.672	FOS	G190H-G270H	1	0.411	0.771	0	—	—	4260

Table 1 — *Continued*

QSO	z_{em} [a]	Instrument	Grating	Search Path			Statistical Path			Proposal ID
				F_{search} [b]	Min z	Max z	F_{stat} [c]	Min z	Max z	
J0120+2133	1.493	FOS	G270H-G190H	1	0.833	1.592	1	0.833	1.468	4396,5664,6109
		FOS	G160L	1	0.620	0.832	1	0.620	0.832	4396
J0121−2820	0.116	COS	G130M-G160M	1	0.010	0.215	1	0.010	0.104	12204
J0122−0421	1.925	FOS	G190H-G270H	1	0.833	1.695	0	—	—	6577,6589
J0122+1339	3.063	STIS	G140L	0	—	—	1	—	—	9067
J0122−2843	0.434	COS	G130M-G160M	1	0.010	0.479	1	0.010	0.419	12204
J0123−0058	1.549	STIS	G230L	1	0.867	1.590	0	—	—	9382
J0123−5848	0.047	COS	G130M-G160M	1	0.010	0.146	1	0.010	0.036	12604
		FOS	G130H-G190H-G270H	1	—	—	1	—	—	4045
J0125−0006	1.070	COS	G160M	1	0.158	0.477	2	0.158	0.477	13398
		FOS	G190H-G270H	1	0.478	1.169	1	0.478	1.049	2424
J0126−2222	0.717	STIS	G230L	1	0.375	0.816	1	0.375	0.699	8225
J0126−0105	1.609	STIS	G230L	1	0.677	1.597	0	—	—	9382
J0127−0619	0.005	FOS	G190H	1	—	—	1	—	—	5408
J0128−3029	0.475	STIS	G140L	1	0.010	0.411	1	0.010	0.411	9506
J0132+0116	1.786	STIS	G230L	0	—	—	0	—	—	9382
J0134+0051	1.522	STIS	G230L	1	0.855	1.597	0	—	—	9382
J0136+2057	0.425	FOS	G190H-G270H	1	0.380	0.524	1	0.380	0.410	3858
J0137−2430	0.831	STIS	G230L	1	0.350	0.930	1	0.350	0.812	8225
J0138−0005	1.340	STIS	G230L	1	0.701	1.439	0	—	—	9382
J0139−0023	1.384	STIS	G230L	1	0.608	1.483	0	—	—	9382
J0139+0619	0.396	STIS	G230L	1	0.010	0.495	1	0.010	0.382	9894
J0139+0131	0.260	FOS	G270H-G190H-G130H	1	0.010	0.359	1	0.010	0.247	5441
J0141−0024	2.611	STIS	G230L	1	1.447	1.598	0	—	—	9051
J0141+1340	0.045	COS	G130M	1	0.010	0.145	1	0.010	0.034	12275
J0144+3411	1.450	FOS	G160L	1	0.113	0.994	0	—	—	6577
J0145−0120	3.124	FOS	G270H	1	1.023	1.695	0	—	—	6577
J0145−3520	0.446	STIS	G230L	1	0.291	0.545	1	0.291	0.431	9507
J0148+3854	1.442	FOS	G160L	1	0.335	1.065	1	0.335	1.065	4396
J0152−2001	2.139	FOS	G270H-G190H	1	0.993	1.695	1	0.993	1.695	3199
		FOS	G160L	1	0.113	0.992	1	0.113	0.992	3051
J0152+0023	0.589	STIS	G230L	1	0.388	0.688	0	—	—	9382
J0153+0052	1.162	STIS	G230L	1	0.571	1.262	0	—	—	9382
J0153+0009	0.837	STIS	G230L	1	0.452	0.936	0	—	—	9382
J0154+0448	0.404	COS	G130M	1	0.010	0.211	0	—	—	12536
J0155−4506	0.451	COS	G130M-G160M	1	0.010	0.476	1	0.010	0.436	11541
J0155−0857	0.164	COS	G130M-G160M	1	0.010	0.264	2	0.010	0.153	12248
J0157−0048	1.545	STIS	G230L	1	0.843	1.604	0	—	—	9382
J0157−0106	3.562	STIS	G140L	0	—	—	1	—	—	9067
J0159+0023	0.163	COS	G130M	1	0.010	0.208	1	0.010	0.151	12569
J0159+1345	0.503	COS	G130M	1	0.010	0.208	2	0.010	0.208	12603
J0201−1132	0.669	COS	G130M-G160M	1	0.010	0.474	1	0.010	0.474	12038
		FOS	G190H-G270H	1	0.475	0.768	1	0.475	0.652	5664
J0202−7620	0.389	COS	G130M-G160M	1	0.010	0.457	1	0.010	0.375	12263
J0208−0503	1.850	STIS	G230L	1	0.752	1.601	0	—	—	9051
J0209−3939	2.813	FOS	G270H	1	1.627	1.695	1	1.627	1.695	6093
J0209−0438	1.130	COS	G130M-G160M	1	0.049	0.480	2	0.049	0.480	12264
J0210−0152	2.370	STIS	G230L	1	—	—	0	—	—	9051
J0212−0737	0.173	COS	G130M-G160M	1	0.010	0.273	2	0.010	0.162	12248
J0217+1104	0.408	FOS	G270H-G190H	1	0.370	0.507	1	0.370	0.393	5441
J0222+4221	1.181	COS	G130M	1	0.010	0.179	2	0.010	0.179	12904
J0222+4302a	0.340	COS	G130M-G160M	1	0.010	0.439	1	0.010	0.326	12863
J0222+4302b	0.444	FOS	G270H-G190H-G130H	1	0.010	0.543	0	—	—	4061
J0226+0015	0.615	COS	G130M-G160M	1	0.010	0.477	2	0.010	0.477	11598
J0228−4057	0.493	COS	G130M-G160M	1	0.010	0.476	1	0.010	0.476	11541
J0230−0859	0.016	COS	G130M-G160M	1	0.010	0.116	1	—	—	12212
J0231+1322	2.065	FOS	G160L	0	—	—	0	—	—	6577
J0232+3423	1.238	STIS	G230L	0	—	—	0	—	—	8569
J0234−0847	0.043	COS	G130M-G160M	1	0.010	0.142	1	0.010	0.032	12953
J0235−0401	1.450	FOS	G270H-G190H	1	0.829	1.549	1	0.829	1.425	4799,5664
J0235−0402	1.438	COS	G130M-G160M	1	0.010	0.480	1	0.010	0.480	11741
		FOS	G160L	1	0.516	1.065	1	0.516	1.065	4799
J0240−1851	0.631	COS	G130M-G160M	1	0.010	0.476	1	0.010	0.476	11541
		STIS	G140L	1	—	—	1	—	—	9506
J0241+0711	0.027	COS	G130M	1	0.010	0.127	1	0.010	0.017	12275
J0241−1514	2.786	STIS	G230L	1	—	—	0	—	—	8569
J0242−0759	0.375	COS	G130M-G160M	1	0.010	0.474	2	0.010	0.361	12248
J0243−7216	0.102	COS	G130M-G160M	1	0.010	0.201	1	0.010	0.091	12263
J0243−3030	0.670	COS	G130M	1	0.010	0.210	2	0.010	0.210	12988
J0244−2904	0.000	STIS	G140L	0	—	—	1	—	—	8287
J0245−3007	0.340	COS	G130M	1	0.010	0.210	2	0.010	0.210	12988
J0246−3007	0.522	COS	G130M	1	0.010	0.210	2	0.010	0.210	12988
J0248−3038	1.093	COS	G130M	1	0.010	0.210	2	0.010	0.210	12988
J0251+4315	1.310	FOS	G160L	1	0.113	0.994	0	—	—	6577
J0253+0107	1.035	STIS	G230L	1	0.722	1.135	0	—	—	9382

Table 1 — *Continued*

QSO	z_{em} [a]	Instrument	Grating	Search Path			Statistical Path			Proposal ID
				F_{search} [b]	Min z	Max z	F_{stat} [c]	Min z	Max z	
J0253−5441	0.537	STIS	G230L	1	0.294	0.636	1	0.294	0.521	9507
J0255−0818	0.625	COS	G160M	1	0.161	0.459	0	—	—	12593
J0256+0110	1.345	STIS	G230L	1	0.899	1.445	0	—	—	9382
J0256−0126	0.879	FOS	G270H	1	0.835	0.978	1	0.835	0.860	4396
		FOS	G160L	1	0.391	0.834	1	0.391	0.834	4396
J0256−3315a	1.915	FOS	G190H-G270H	1	1.064	1.695	1	1.064	1.695	5320,5631
J0256−3315b	1.863	STIS	G140L	1	0.012	0.411	0	—	—	8569
J0259+0037	0.533	COS	G130M-G160M	1	0.010	0.477	2	0.010	0.477	12248
J0304−0008	3.290	COS	G130M	1	0.067	0.200	0	—	—	12033
		STIS	G230L	1	0.060	1.607	1	0.060	1.607	7272,7575
J0304−2212	1.400	FOS	G270H	1	0.828	1.499	0	—	—	6224
J0307−7250	0.027	COS	G130M-G160M	1	0.010	0.127	1	0.010	0.017	12263
J0308−3250	0.247	STIS	G140L	1	0.020	0.346	1	0.020	0.234	9506
J0310−0049	0.080	COS	G130M-G160M	1	0.010	0.180	2	0.010	0.069	12248
J0311−6039	0.000	STIS	G140L	0	—	—	1	—	—	8287
J0318−2012	2.869	STIS	G230L	1	1.442	1.605	0	—	—	8569
J0319+4130	0.017	COS	G160M	1	—	—	1	—	—	12260
J0329−2357	0.895	STIS	G230L	1	0.871	0.994	1	0.871	0.876	8225
J0336−3607	1.093	FOS	G270H	1	1.027	1.192	1	1.027	1.072	4396
		FOS	G160L	1	0.730	1.026	1	0.730	1.026	4396
J0336+3218	1.258	FOS	G270H	1	1.130	1.357	1	1.130	1.235	5441
J0349−5344	0.130	STIS	G140L	1	0.010	0.229	2	0.010	0.118	9858
J0351−1429	0.614	COS	G130M-G160M	1	0.010	0.462	2	0.010	0.462	13398
		FOS	G190H-G270H	1	0.463	0.713	1	0.463	0.597	2424
J0352−0710	0.962	FOS	G270H	1	0.834	1.061	1	0.834	0.942	4396
J0354−2724	2.823	STIS	G230L	1	—	—	0	—	—	8569
J0355−5451	0.269	STIS	G230L	1	—	—	1	—	—	9507
J0357−4812	1.005	FOS	G270H	1	0.834	1.104	1	0.834	0.985	4396,6103
		FOS	G160L	1	0.720	0.833	1	0.720	0.833	4396,6103
J0401−0540	0.570	COS	G130M-G160M	1	0.010	0.476	2	0.010	0.476	11598
J0405−1308	0.571	FOS	G190H-G270H	1	0.434	0.670	1	0.434	0.555	2578
J0407−1211	0.574	COS	G130M-G160M	1	0.010	0.476	1	0.010	0.476	11541
		FOS	G130H-G190H-G270H	1	0.477	0.673	1	0.477	0.558	1025,3837
J0411−4956	0.817	STIS	G230L	1	0.289	0.916	1	0.289	0.798	9507
J0416−2056	0.807	STIS	G230L	1	0.383	0.907	1	0.383	0.789	8225
J0417−0554	0.781	FOS	G270H-G190H	1	0.346	0.880	1	0.346	0.763	3269,5664
J0423−0120	0.915	FOS	G270H	1	0.882	1.014	1	0.882	0.895	2424,4044,6799
		STIS	G230L	1	0.477	0.881	0	—	—	8569
J0424+0204	2.044	FOS	G270H	1	0.833	1.696	0	—	—	6577
J0426−5712	0.104	COS	G130M-G160M	1	0.010	0.203	2	0.010	0.093	11692
J0427−1303	2.159	FOS	G270H	1	1.299	1.696	0	—	—	6577
J0430−5336	0.039	COS	G130M	1	0.010	0.139	1	0.010	0.029	12275
J0436−5258	1.231	COS	G130M-G160M	1	0.010	0.476	1	0.010	0.476	11520
		STIS	G140L	1	—	—	1	—	—	9506
J0438−2608	0.690	STIS	G230L	2	—	—	1	—	—	9507
J0438−6147	0.069	COS	G130M-G160M	1	0.010	0.168	2	0.010	0.058	11692
J0439−2422	0.840	STIS	G230L	1	0.384	0.940	1	0.384	0.821	8225
J0439−5311	0.243	COS	G130M-G160M	1	0.010	0.342	1	0.010	0.230	11520
		STIS	G140L	1	—	—	1	—	—	9506
J0439−4540	0.224	STIS	G230L	1	0.010	0.323	1	0.010	0.211	9894
J0440−5248	1.053	COS	G130M-G160M	1	0.010	0.476	1	0.010	0.476	11520
		STIS	G140L	1	—	—	1	—	—	9506
J0441−4313	0.593	COS	G130M	1	0.010	0.179	0	—	—	12536
		FOS	G190H-G270H	1	0.343	0.692	1	0.343	0.577	4581
		STIS	G140L	1	0.180	0.342	0	—	—	9382
J0443−2820	0.155	STIS	G230L	1	—	—	1	—	—	9507
J0448+0950	2.110	STIS	G230L	0	—	—	0	—	—	8569
J0448−2044	1.896	FOS	G160L	0	—	—	1	—	—	4396
J0449−3911	1.288	FOS	G160L	1	0.292	1.065	1	0.292	1.065	4396
J0452−1640	2.600	STIS	G230L	1	0.583	1.606	0	—	—	8569
J0452−2953	0.286	FOS	G190H	1	—	—	1	—	—	6799
J0452−2201	0.898	STIS	G230L	1	0.626	0.998	1	0.626	0.879	8225
J0453−1305	2.300	STIS	G230L	1	1.319	1.605	0	—	—	8569
J0455−4216	2.660	FOS	G190H-G270H	1	1.489	1.695	0	—	—	6577
J0456−2159	0.533	COS	G160M	1	0.139	0.446	2	0.139	0.446	12252
		FOS	G130H-G270H-G190H	1	0.069	0.633	0	—	—	1026
J0456+0400	1.345	FOS	G270H-G190H	1	0.428	1.444	0	—	—	5351,5451
J0503−6633	0.064	COS	G130M-G160M	1	0.010	0.163	2	0.010	0.053	11692
J0504−2944	0.552	STIS	G230L	1	0.010	0.651	1	0.010	0.536	9506,9507
J0506−6109	1.093	FOS	G270H	1	0.988	1.192	1	0.988	1.072	4396
J0509−3232	1.567	STIS	G140L	0	—	—	1	—	—	9506
J0514−3326	1.569	STIS	G230L	1	0.615	1.611	0	—	—	9165
J0538−4405	0.894	FOS	G130H-G270H	1	0.878	0.993	1	—	—	4396
J0552−6402	0.680	COS	G130M-G160M	1	0.010	0.438	2	0.010	0.438	11692
J0559−5026	0.137	COS	G130M-G160M	1	0.010	0.236	2	0.010	0.125	11692

Table 1 — *Continued*

QSO	z_{em} [a]	Instrument	Grating	Search Path			Statistical Path			Proposal ID
				F_{search} [b]	Min z	Max z	F_{stat} [c]	Min z	Max z	
J0612−1415	0.035	COS	G130M	0	—	—	1	—	—	12275
J0623−6436	0.129	COS	G130M-G160M	1	0.010	0.228	2	0.010	0.117	11692
J0630+6904	0.374	FOS	G130H-G190H-G270H	1	0.010	0.473	1	0.010	0.360	3791,4112,4818,5664
J0635−7516	0.656	COS	G130M-G160M	1	0.010	0.438	2	0.010	0.438	11692
		FOS	G190H-G270H	1	0.439	0.755	1	0.439	0.639	4044
J0713+1146	0.768	FOS	G190H-G270H	1	0.426	0.867	1	0.426	0.750	2578
J0714+7408	0.371	COS	G130M	1	0.010	0.206	1	0.010	0.206	12275
J0719+7427	0.475	COS	G130M	1	0.010	0.206	1	0.010	0.206	12275
J0721+7120	0.300	COS	G130M-G160M	1	0.010	0.399	1	0.010	0.287	12025
J0732+6159	0.325	STIS	G140L	1	0.010	0.411	1	0.010	0.311	9506
J0739+8146	1.024	STIS	G230L	1	0.571	1.123	0	—	—	8569
J0741+3111	0.630	FOS	G160L	1	0.115	0.729	0	—	—	6577
J0743−6726	1.511	FOS	G270H-G190H	1	0.829	1.610	1	0.829	1.485	5225,6109
J0744+3753	1.063	FOS	G270H	1	0.942	1.162	1	0.942	1.042	2578
J0744+3208	1.051	STIS	G230L	0	—	—	0	—	—	9051
J0745+3143	0.462	FOS	G190H-G270H	1	0.387	0.561	1	0.387	0.447	3791
J0749+4152	3.105	STIS	G140L	0	—	—	1	—	—	9067
J0751+2919	0.914	COS	G130M-G160M	1	0.010	0.480	1	0.010	0.480	11741
J0753+4231	3.590	STIS	G140L	0	—	—	1	—	—	9067
J0800+4435	2.505	STIS	G140L	0	—	—	1	—	—	9067
J0800+3051	4.666	STIS	G230L	0	—	—	0	—	—	9759
J0801+5210	3.234	STIS	G140L	0	—	—	1	—	—	9506
J0803+4332	0.448	COS	G130M-G160M	1	0.010	0.476	2	0.010	0.434	11598
J0804+6459	0.148	STIS	G140L	2	—	—	1	—	—	7617
J0806+5041	2.432	STIS	G230L	1	0.784	1.599	0	—	—	9051
J0808+0514	0.360	COS	G130M	1	0.010	0.206	2	0.010	0.206	12603
J0809+4619	0.657	COS	G130M-G160M	1	0.010	0.477	2	0.010	0.477	12248
J0810+7602	0.100	COS	G130M-G160M	1	0.010	0.199	1	0.010	0.089	11686
J0813+4813	3.163	FOS	G160L	1	—	—	0	—	—	5351,3939,1193
J0814+5029	3.883	STIS	G140L	0	—	—	1	—	—	9067
J0820+2334	0.470	COS	G130M-G160M	1	0.010	0.476	2	0.010	0.455	11598
J0825+5127	3.511	STIS	G140L	0	—	—	1	—	—	9067
J0826−2230	0.910	FOS	G270H	1	0.828	1.009	0	—	—	6577
J0826+0742	0.310	COS	G130M-G160M	1	0.010	0.410	2	0.010	0.297	12248
J0827+1052	2.295	STIS	G230L	1	—	—	0	—	—	8569
J0830+2410	0.939	FOS	G270H	1	0.856	1.038	1	0.856	0.919	5441
		FOS	G160L	1	0.113	0.855	0	—	—	6577
J0835+2459	0.331	COS	G130M-G160M	1	0.010	0.430	1	0.010	0.317	12025
J0838+5406	0.029	COS	G160M	1	—	—	1	—	—	12557
J0839+5256	1.545	STIS	G140L	1	—	—	1	—	—	9067
J0840+1312	0.684	FOS	G190H-G270H	1	0.421	0.783	1	0.421	0.667	2578
J0843+4117	0.990	COS	G130M-G160M	1	0.010	0.476	2	0.010	0.476	12248
J0844+7653	0.131	COS	G130M-G160M	1	0.010	0.231	1	0.010	0.120	11520
J0845+1328	1.877	FOS	G160L	1	0.113	0.994	0	—	—	6577
J0847+3445	0.064	COS	G130M	1	0.010	0.163	1	0.010	0.053	12569
		FOS	G130H-G270H	1	—	—	2	—	—	2717
J0851+1612	1.936	FOS	G270H	1	1.200	1.697	1	1.200	1.697	6589
J0852+0313	0.297	COS	G130M	1	0.010	0.210	2	0.010	0.210	12603
J0853+4349	0.513	COS	G130M	1	0.010	0.124	2	0.010	0.124	13398
		FOS	G190H-G270H	1	0.366	0.612	1	0.366	0.497	2424
		FOS	G160L	1	0.279	0.365	1	0.279	0.365	2424
J0854+2006	0.306	FOS	G130H-G190H-G270H	1	—	—	1	—	—	3201,4817,5664
J0857+1855	1.892	STIS	G140L	0	—	—	0	—	—	8569
J0859+4637	0.923	FOS	G160L	1	0.496	1.022	1	0.496	0.903	4952
J0902−1415	1.327	FOS	G270H	1	0.889	1.426	1	0.889	1.303	3858
J0904+1309	0.000	STIS	G140L	0	—	—	1	—	—	8287
J0906+1646	0.411	FOS	G190H-G270H	1	0.376	0.510	1	0.376	0.396	2578
J0909+3236	0.808	COS	G130M	1	0.010	0.210	2	0.010	0.210	12603
J0909−0932	0.625	FOS	G270H	1	—	—	2	—	—	6548
J0909+4254	0.670	FOS	G190H-G270H	1	0.655	0.769	1	—	—	3858
J0910+1014	0.463	COS	G130M-G160M	1	0.010	0.477	2	0.010	0.448	11598
J0912+2450	0.654	STIS	G140L	1	0.011	0.410	1	0.011	0.410	9506
J0912+2957	0.305	COS	G130M-G160M	1	0.010	0.405	2	0.010	0.292	12248
J0914+0837	0.648	COS	G130M	1	0.010	0.210	2	0.010	0.210	12603
J0914+2823	0.735	COS	G130M-G160M	1	0.010	0.476	2	0.010	0.476	11598
J0915+4756	3.336	COS	G130M	1	0.010	0.124	0	—	—	12816
J0915+4426	3.944	STIS	G140L	0	—	—	0	—	—	9759
J0919+5521	0.122	COS	G130M-G160M	1	0.010	0.222	1	0.010	0.111	12029
J0919+5105	0.553	FOS	G190H-G270H	1	0.345	0.652	1	0.345	0.537	2424
		FOS	G160L	1	0.299	0.344	1	0.299	0.344	2424
J0925+4535	0.329	COS	G130M-G160M	1	0.010	0.429	2	0.010	0.316	12248
J0925+4004	0.470	COS	G130M-G160M	1	0.010	0.476	2	0.010	0.456	11598
J0925+1954	0.192	COS	G130M	1	0.010	0.193	1	0.010	0.180	12569
J0926+3055	4.190	STIS	G140L	0	—	—	1	—	—	8582
J0927+3902	0.699	FOS	G190H-G270H	1	0.355	0.798	1	0.355	0.682	2578,4052

Table 1 — *Continued*

QSO	z_{em} [a]	Instrument	Grating	Search Path			Statistical Path			Proposal ID
				F_{search} [b]	Min z	Max z	F_{stat} [c]	Min z	Max z	
J0928+6025	0.295	COS	G130M-G160M	1	0.010	0.395	2	0.010	0.282	11598
J0929+4644	0.240	COS	G130M-G160M	1	0.010	0.340	2	0.010	0.227	12248
J0930+2848	0.486	COS	G130M	1	0.010	0.210	2	0.010	0.210	12603
J0931+2628	0.778	COS	G130M	1	0.010	0.210	2	0.010	0.210	12603
J0935+0204	0.659	COS	G130M-G160M	1	0.010	0.476	2	0.010	0.476	11598
J0936+3207	1.149	COS	G130M	1	0.010	0.206	2	0.010	0.206	12603
J0937+1700	0.506	COS	G130M	1	0.010	0.207	2	0.010	0.207	12603
J0937+7301	2.528	FOS	G270H	1	1.516	1.695	0	—	—	6577
J0938+4128	1.937	FOS	G270H	1	0.856	1.696	1	0.856	1.696	5664,6237
J0943+0531	0.564	COS	G130M-G160M	1	0.010	0.476	2	0.010	0.476	11598
J0944+2554	2.910	STIS	G230L	1	1.472	1.592	0	—	—	8569
J0946+4711	0.230	COS	G130M-G160M	1	0.010	0.330	2	0.010	0.218	12248
J0947+1005	0.138	COS	G130M-G160M	1	0.010	0.238	2	0.010	0.127	12248
J0948+4323	1.892	STIS	G230L	1	0.804	1.598	0	—	—	9051
J0948+4039	1.252	FOS	G270H	1	0.901	1.351	1	0.901	1.229	5441
J0949+5445	1.376	COS	G160M	1	0.142	0.440	0	—	—	12593
J0949−0514	1.098	COS	G160M	1	0.167	0.460	0	—	—	12593
J0949+2955	1.221	STIS	G230L	2	—	—	0	—	—	8284,3200
J0949+3902	0.360	COS	G130M-G160M	1	0.010	0.459	2	0.010	0.346	12248
J0950+4831	0.588	COS	G130M-G160M	1	0.010	0.429	2	0.010	0.429	11598
J0950+5846	0.151	STIS	G140L	0	—	—	1	—	—	9067
J0950+5801	3.970	STIS	G140L	0	—	—	1	—	—	8582
J0951+3307	0.644	COS	G130M	1	0.012	0.210	2	0.012	0.210	12486
J0951+3542	0.400	COS	G130M	1	0.010	0.210	2	0.010	0.210	12603
J0953−0038	1.382	STIS	G230L	1	0.550	1.481	0	—	—	9382
J0954+1743	1.478	FOS	G160L	1	0.114	1.063	0	—	—	6577
J0955+5940	4.340	STIS	G140L	0	—	—	1	—	—	9067
J0956−0453	0.150	COS	G130M	1	0.010	0.206	1	0.010	0.138	12275
J0956+4115	0.234	COS	G130M-G160M	1	0.010	0.334	1	0.010	0.221	12038
		FOS	G190H-G270H-G130H	1	—	—	1	—	—	1018,3220
J0957+5440	2.584	FOS	G270H	1	1.649	1.695	0	—	—	6577
J0957+5522	0.909	FOS	G190H-G270H	1	0.437	1.008	1	0.437	0.889	4052
J0958+3224	0.530	FOS	G270H-G190H-G130H	1	0.143	0.630	1	0.143	0.514	3566,4952,5451
		STIS	G140L	1	0.010	0.142	1	0.010	0.142	9506
J0958+5550	1.021	COS	G160M	0	—	—	0	—	—	12593
J0959+3203	0.563	COS	G130M	1	0.010	0.205	2	0.010	0.205	12603
J0959+0503	0.161	COS	G130M-G160M	1	0.010	0.261	2	0.010	0.150	12248
J1000+0005	0.905	STIS	G230L	1	0.291	1.005	0	—	—	8569
J1001+5944	0.746	COS	G130M-G160M	1	0.010	0.476	2	0.010	0.476	12248
J1001+5553	1.415	FOS	G270H	1	0.830	1.514	1	0.830	1.390	5683,5781
		FOS	G270H	1	—	—	1	—	—	5683,5781
		STIS	G230L	1	0.808	0.829	0	—	—	8336,5683
		FOS	G160L	1	0.113	0.807	0	—	—	8336,5683
J1001+5454	1.750	FOS	G270H	1	1.058	1.697	1	1.058	1.697	5664
		FOS	G160L	1	0.993	1.057	0	—	—	6577
J1001+5610	3.216	STIS	G140L	0	—	—	1	—	—	8582
J1001+2847	0.185	FOS	G190H-G270H	1	—	—	1	—	—	6616
J1002+3240	0.828	COS	G130M	1	0.010	0.210	2	0.010	0.210	12603
J1003+6813	0.773	FOS	G190H-G270H	1	0.367	0.872	1	0.367	0.755	3791
		FOS	G160L	1	—	—	1	—	—	3791
J1004+2855	0.329	COS	G130M-G160M	1	0.010	0.428	1	0.010	0.315	12038
		FOS	G130H-G190H-G270H	1	—	—	1	—	—	3418,4044
J1004+0513	0.161	FOS	G270H-G190H-G130H	1	0.010	0.260	1	0.010	0.149	6247,6781
J1004+2225	0.974	FOS	G270H	1	0.929	1.073	1	0.929	0.954	5441
J1005+0134	1.077	COS	G130M-G160M	1	0.010	0.480	2	0.010	0.480	12264
J1007+0042	1.681	STIS	G230L	0	—	—	0	—	—	9382
J1007+1248	0.240	COS	G130M	1	0.010	0.193	1	0.010	0.193	12569
		STIS	G230L	1	—	—	1	—	—	9432
J1007+3638	1.034	COS	G160M	1	0.162	0.459	0	—	—	12593
J1008−0223	0.000	STIS	G140L	0	—	—	1	—	—	9067
J1008−0018	1.350	STIS	G230L	1	0.497	1.449	0	—	—	9382
J1009+0713	0.455	COS	G130M-G160M	1	0.023	0.476	2	0.023	0.441	11598
J1009−1226	0.693	STIS	G230L	1	0.289	0.792	1	0.289	0.676	9507
J1009−0026	1.244	STIS	G230L	1	0.532	1.343	0	—	—	9382
J1009+0036	1.702	STIS	G230L	1	0.686	1.590	0	—	—	9382
J1010+3003	0.255	COS	G130M-G160M	1	0.010	0.355	1	0.010	0.243	12025
J1010+0003	1.399	STIS	G230L	1	0.732	1.498	0	—	—	9382
J1010+4132	0.611	FOS	G190H-G270H	1	0.340	0.710	1	0.340	0.594	3791
		FOS	G160L	1	0.305	0.339	1	0.305	0.339	3791
J1010−0047	1.671	STIS	G230L	1	0.770	1.594	0	—	—	9382
J1011+1304	1.287	FOS	G270H	1	0.830	1.386	1	0.830	1.264	4581,4952
		FOS	G160L	1	0.437	0.829	1	0.437	0.829	4952
J1013+3551	0.070	COS	G130M	1	0.010	0.169	1	0.010	0.059	12275
		FOS	G130H	1	—	—	1	—	—	3065
J1013+0500	0.265	COS	G130M	1	0.010	0.210	2	0.010	0.210	12603

Table 1 — *Continued*

QSO	z_{em} [a]	Instrument	Grating	Search Path			Statistical Path			Proposal ID
				F_{search} [b]	Min z	Max z	F_{stat} [c]	Min z	Max z	
J1013+5615	3.613	STIS	G140L	0	—	—	1	—	—	8582
J1014−0418	0.058	COS	G130M-G160M	1	0.010	0.157	1	0.010	0.047	11524
J1014+4300	3.125	STIS	G140L	0	—	—	1	—	—	8287
J1016+4706	0.821	COS	G130M-G160M	1	0.010	0.430	2	0.010	0.430	11598
J1017+5924	0.850	COS	G160M	1	0.162	0.459	0	—	—	12593
J1017+5356	1.400	STIS	G230L	1	0.757	1.499	0	—	—	9051
J1019+2743	1.928	FOS	G270H	1	0.968	1.695	1	0.968	1.695	5664
J1021+3437	1.405	COS	G160M	1	0.231	0.460	0	—	—	12593
J1022+0132	0.789	COS	G130M-G160M	1	0.010	0.476	2	0.010	0.476	11598
J1022+3041	1.317	STIS	G140L	1	0.014	0.411	0	—	—	8569
J1022+3931	0.603	COS	G160M	1	0.162	0.460	0	—	—	12593
J1022+0101	1.563	STIS	G230L	1	0.929	1.593	0	—	—	9382
J1024+1912	0.828	FOS	G160L	1	0.312	0.927	1	0.312	0.809	2424
J1026+6136	3.848	STIS	G140L	0	—	—	1	—	—	9067
J1026+6746	1.181	STIS	G140L	0	—	—	1	—	—	9506
J1027+1834	2.840	COS	G130M	1	0.010	0.124	0	—	—	12816
J1028−0100a	1.437	FOS	G270H	1	0.830	1.536	1	0.830	1.412	6819
J1028−0100b	1.530	FOS	G270H	1	0.834	1.629	1	0.834	1.504	6819
		STIS	G230L	1	0.397	0.833	0	—	—	9382
J1031+3102	0.178	FOS	G270H-G190H	1	—	—	2	—	—	5934
J1031+5053	0.361	COS	G130M-G160M	1	0.010	0.460	1	0.010	0.347	12025
		STIS	G140L	1	—	—	1	—	—	9506
J1031−0036	1.258	STIS	G230L	0	—	—	0	—	—	9382
J1032+5051	0.173	COS	G130M-G160M	1	0.010	0.273	1	0.010	0.161	12025
		STIS	G140L	1	—	—	1	—	—	9506
J1032+6502	0.005	COS	G160M	1	—	—	1	—	—	12557
J1032+0003	1.190	STIS	G230L	1	0.652	1.289	0	—	—	9382
J1033+2112	0.315	COS	G130M	1	0.010	0.210	2	0.010	0.210	12603
J1037+0028	1.733	STIS	G230L	1	0.871	1.594	0	—	—	9382
J1038−2752	2.168	FOS	G160L	0	—	—	0	—	—	6577
J1040+1053	0.136	COS	G130M	0	—	—	2	—	—	12533
J1040+5145	4.045	STIS	G140L	0	—	—	0	—	—	9759
J1041+0610	1.270	COS	G160M	1	0.149	0.452	2	0.149	0.452	12252
		FOS	G270H	1	0.829	1.369	1	0.829	1.247	2424,5664
		FOS	G160L	1	0.453	0.828	1	0.453	0.828	2424
J1042+1203	1.028	FOS	G160L	1	0.433	1.065	1	0.433	1.007	2424
J1047+1304	0.399	COS	G130M	1	0.010	0.187	1	0.010	0.187	12198
J1047−0047	0.740	STIS	G230L	1	0.418	0.839	0	—	—	9382
J1048+1207	0.291	COS	G130M	1	0.010	0.187	1	0.010	0.187	12198
J1048+1306	0.218	COS	G130M-G160M	1	0.010	0.318	1	0.010	0.206	12198
J1048+0032	1.649	STIS	G230L	1	0.690	1.591	0	—	—	9382
J1050+5447	2.165	FOS	G270H	1	0.990	1.696	0	—	—	5948
J1051+1247	1.281	COS	G130M	0	—	—	2	—	—	12603
J1051+3359	0.167	COS	G130M-G160M	1	0.010	0.267	2	0.010	0.155	12024
J1051−0051	0.357	COS	G130M-G160M	1	0.010	0.456	2	0.010	0.343	12248
		FOS	G190H-G270H	1	—	—	1	—	—	2424
		STIS	G140L	1	—	—	2	—	—	7295
J1052+6125	0.421	FOS	G160L	1	0.114	0.520	0	—	—	6577
J1054−0020	1.021	STIS	G230L	1	0.290	1.120	0	—	—	9382
J1057−0139	0.000	STIS	G140L	0	—	—	1	—	—	9067
J1058+1951	1.110	FOS	G270H	1	1.019	1.209	1	1.019	1.088	2424,5441
		FOS	G160L	1	0.535	1.018	1	0.535	1.018	2424
J1059+0519	0.754	COS	G130M	1	0.010	0.210	2	0.010	0.210	12603
J1059+1441	0.630	COS	G130M-G160M	1	0.010	0.476	2	0.010	0.476	12248
J1059+1211	0.992	COS	G130M	1	0.010	0.207	2	0.010	0.207	12603
J1059+2517	0.662	COS	G130M-G160M	1	0.010	0.477	2	0.010	0.477	12248
J1100+1046	0.421	COS	G130M	1	0.010	0.205	2	0.010	0.205	12603
J1103+4141	0.401	COS	G130M-G160M	1	0.010	0.476	2	0.010	0.387	12248
J1103−2645	2.145	FOS	G270H	1	1.138	1.695	1	1.138	1.695	5664
J1103−3251	0.354	COS	G130M	1	0.010	0.206	1	0.010	0.206	12275
J1103−2329	0.186	COS	G130M-G160M	1	0.010	0.285	1	0.010	0.174	12025
J1103+3715	1.294	STIS	G230L	1	0.933	1.394	0	—	—	9051
J1104+3141	0.434	COS	G130M-G160M	1	0.010	0.457	2	0.010	0.420	12248
J1104+7658	0.311	FOS	G190H-G270H-G130H	1	0.010	0.410	1	0.010	0.297	2424,4939
J1104−1016	0.186	STIS	G230L	1	—	—	1	—	—	9507
J1104+3812	0.030	COS	G130M-G160M	1	0.010	0.130	1	0.010	0.020	11520
J1105+3425	0.509	COS	G130M-G160M	1	0.010	0.476	1	0.010	0.476	11541
J1106+6400	2.190	FOS	G270H-G190H	1	0.347	1.696	1	0.347	1.696	5950
J1106−0052	0.425	FOS	G190H-G270H	1	0.402	0.524	1	0.402	0.410	3858
		STIS	G140L	1	0.077	0.401	2	0.077	0.401	7295
J1106−1821	2.303	FOS	G270H	1	1.006	1.695	0	—	—	5951
		FOS	G270H	1	1.002	1.005	0	—	—	5951
J1106+7234	0.008	COS	G130M-G160M	1	0.010	0.108	1	—	—	12212
J1107+1628	0.634	FOS	G190H-G270H	1	0.342	0.733	1	0.342	0.617	3791
		FOS	G160L	1	—	—	1	—	—	3791

Table 1 — *Continued*

QSO	z_{em} [a]	Instrument	Grating	Search Path			Statistical Path			Proposal ID
				F_{search} [b]	Min z	Max z	F_{stat} [c]	Min z	Max z	
J1107+0048	1.390	STIS	G230L	1	0.502	1.490	0	—	—	9382
J1107+0003	1.726	STIS	G230L	1	0.788	1.590	0	—	—	9382
J1108+3133	2.243	STIS	G230L	1	0.884	1.599	0	—	—	9051
J1108−0802	0.340	STIS	G230L	1	—	—	1	—	—	9507
J1109+0051	0.957	STIS	G230L	1	0.423	1.056	0	—	—	9382
J1110+4831	2.960	STIS	G140L	0	—	—	1	—	—	9506
J1110+3019	1.521	STIS	G230L	1	0.795	1.593	0	—	—	9051
J1110+0048	0.761	STIS	G230L	0	—	—	0	—	—	9382
J1111+5547	0.765	COS	G130M-G160M	1	0.010	0.480	1	0.010	0.480	12025
J1112+3539	0.635	COS	G130M-G160M	1	0.010	0.476	2	0.010	0.476	11598
J1112+0013	1.433	STIS	G230L	1	0.290	1.532	0	—	—	9382
J1114+4037	0.734	FOS	G190H-G270H	1	0.406	0.833	1	0.406	0.716	2578
J1115+4249	0.300	COS	G130M	1	0.010	0.207	1	0.010	0.207	12275
J1115+0237	0.566	COS	G130M	1	0.010	0.210	2	0.010	0.210	12603
J1117+4413	0.144	FOS	G130H-G270H-G190H	1	0.010	0.243	1	0.010	0.132	6484,6781
J1117+2634	0.422	COS	G130M-G160M	1	0.010	0.457	2	0.010	0.407	12248
J1118+0746	1.722	FOS	G270H	1	0.830	1.696	1	0.830	1.694	5681,6222
		FOS	G270H	1	1.697	1.697	1	—	—	5681,6222
J1118+0745	1.735	COS	G130M	1	0.010	0.210	2	0.010	0.210	12603
J1118+4025	0.154	COS	G130M-G160M	1	0.010	0.254	2	0.010	0.143	11519
		FOS	G130H-G270H-G190H	1	—	—	1	—	—	6781
J1119+2119	0.176	COS	G130M-G160M	1	0.010	0.276	1	0.010	0.164	12038
		FOS	G190H-G270H-G130H	1	—	—	1	—	—	4115,6781
J1119+6004	2.638	STIS	G140L	0	—	—	1	—	—	9506
J1120+0413	0.545	COS	G130M	1	0.010	0.210	2	0.010	0.210	12603
J1120−4315	0.056	COS	G130M	1	0.010	0.156	1	0.010	0.046	12275
J1121+0325	0.152	COS	G130M-G160M	1	0.010	0.252	2	0.010	0.140	12248
J1121+1236	0.685	FOS	G190H-G270H	1	0.428	0.784	1	0.428	0.668	5441
J1122+0318	0.474	COS	G130M	1	0.010	0.210	2	0.010	0.210	12603
J1122+5755	0.900	COS	G130M-G160M	1	0.010	0.476	2	0.010	0.476	12248
J1124+4201	0.234	COS	G130M-G160M	1	0.010	0.333	2	0.010	0.221	12024
		FOS	G190H	1	—	—	1	—	—	5456
J1124−1705	2.400	FOS	G270H-G190H	1	0.347	1.696	1	0.347	1.696	5950
J1125+5910	0.852	COS	G130M-G160M	1	0.010	0.476	1	0.010	0.476	11520
		STIS	G140L	1	—	—	1	—	—	4952,9874
		FOS	G160L	1	0.548	0.952	1	0.548	0.833	4952,9874
J1126+0034	1.783	STIS	G230L	1	1.111	1.593	0	—	—	9382
J1126+3918	1.470	FOS	G160L	0	—	—	1	—	—	4952
J1126+5134	0.026	COS	G160M	0	—	—	1	—	—	12557
J1126−0141	0.046	COS	G130M	1	0.012	0.146	1	0.012	0.036	12275
J1127+2654	0.378	COS	G130M	1	0.010	0.205	2	0.010	0.205	12603
		FOS	G270H	1	—	—	2	—	—	6548
J1129−0424	0.060	COS	G130M	1	0.010	0.159	1	0.010	0.049	12569
J1129−1941	0.918	STIS	G140L	0	—	—	1	—	—	9506
J1130−1449	1.187	FOS	G190H-G270H	1	0.836	1.286	0	—	—	3483,3858,6577
		FOS	G160L	1	0.165	0.835	0	—	—	6577
J1131+3114	0.290	COS	G130M-G160M	1	0.010	0.390	2	0.010	0.277	11519
J1131+1556	0.182	COS	G130M	1	0.010	0.206	2	0.010	0.171	12603
J1132+1335	0.200	COS	G130M	1	0.010	0.210	2	0.010	0.188	12603
J1133+0327	0.525	COS	G130M-G160M	1	0.010	0.430	2	0.010	0.430	13033
J1133+1052	0.510	FOS	G190H-G270H	1	0.365	0.609	1	0.365	0.494	2424
J1134+2555	0.709	COS	G130M-G160M	1	0.010	0.447	2	0.010	0.447	12248
J1135−0318	0.237	FOS	G190H	1	—	—	1	—	—	5456
J1137+3907	1.026	STIS	G230L	2	—	—	0	—	—	9051
J1139−3744	0.009	COS	G130M-G160M	1	0.010	0.109	1	—	—	12212
J1139−1351	0.557	COS	G130M	1	0.010	0.206	1	0.010	0.206	12275
		FOS	G190H-G270H	1	0.352	0.656	1	0.352	0.541	2424
		FOS	G160L	1	0.334	0.351	1	0.334	0.351	2424
J1139+6547	0.652	COS	G130M-G160M	1	0.010	0.476	1	0.010	0.476	11541
		FOS	G190H-G270H	1	0.477	0.751	1	0.477	0.635	2424,2578,4044
J1141+0147	0.383	FOS	G190H	1	0.357	0.482	1	0.357	0.369	5456
J1142+3016	0.481	COS	G130M	1	0.010	0.207	2	0.010	0.207	12603
J1143+3452	3.130	STIS	G140L	0	—	—	1	—	—	8287
J1147−0132	0.382	FOS	G190H	1	0.377	0.481	1	—	—	5852
J1148+1050	1.010	FOS	G190H	1	0.387	0.901	1	0.387	0.901	5852
J1148+1048	1.010	FOS	G190H	1	0.427	0.902	1	0.427	0.902	5852
J1148+1047	1.100	FOS	G190H	1	0.365	0.902	1	0.365	0.902	5852
J1150−0023	1.980	FOS	G160L	1	0.135	1.065	1	0.135	1.065	5095
J1151+5437	0.975	COS	G130M-G160M	1	0.010	0.480	1	0.010	0.480	11741
		FOS	G190H-G270H-G130H	1	0.481	1.075	1	0.481	0.955	4952,6220
J1151+3825	1.304	FOS	G160L	1	0.174	1.063	0	—	—	6577
J1153+4931	0.334	FOS	G270H-G190H	1	0.298	0.433	1	0.298	0.320	5441
J1155+2922	0.520	COS	G130M	1	0.010	0.210	2	0.010	0.210	12603
J1157−0022	0.260	COS	G130M-G160M	1	0.010	0.360	2	0.010	0.247	11598
J1158+6254	0.594	FOS	G270H	1	—	—	1	—	—	4952

Table 1 — *Continued*

QSO	z_{em} [a]	Instrument	Grating	Search Path			Statistical Path			Proposal ID
				F_{search} [b]	Min z	Max z	F_{stat} [c]	Min z	Max z	
J1159+2107	0.349	FOS	G270H-G190H	1	0.298	0.448	1	0.298	0.335	5441
J1159+2915	0.729	FOS	G190H-G270H	1	0.354	0.828	1	0.354	0.711	3791,5441
J1200+3126	2.970	STIS	G140L	0	—	—	1	—	—	8287
J1201+0111	0.000	STIS	G140L	0	—	—	2	—	—	9874
J1201−1354	0.506	COS	G130M	1	0.010	0.206	1	0.010	0.206	12275
J1203+4431	0.002	COS	G130M-G160M	1	0.010	0.102	1	—	—	11834
J1203+1522	2.970	STIS	G140L	0	—	—	1	—	—	8287
J1204+2754	0.164	COS	G130M-G160M	1	0.010	0.264	2	0.010	0.152	12248
		FOS	G190H-G270H-G130H	0	—	—	1	—	—	4115
J1204−4343	0.014	COS	G130M	1	0.010	0.114	1	—	—	12275
J1205−2634	0.786	STIS	G230L	1	0.502	0.885	1	0.502	0.768	8225
J1205+1042	1.088	COS	G130M	1	0.010	0.187	2	0.010	0.187	11698
J1207+2624	0.323	COS	G130M-G160M	1	0.010	0.423	2	0.010	0.310	12248
J1208+4540	1.158	COS	G130M-G160M	1	0.010	0.480	1	0.010	0.480	11741
		FOS	G190H-G270H	1	0.481	1.257	1	0.481	1.136	2424
		FOS	G160L	1	—	—	1	—	—	2424
J1209+1036	0.394	COS	G130M	1	0.050	0.187	2	0.050	0.187	11698
J1209+0232	0.238	STIS	G140L	1	0.012	0.338	2	0.012	0.225	9874
J1209−0501	0.128	COS	G130M	0	—	—	2	—	—	12533
J1210+3157	0.388	COS	G130M-G160M	1	0.010	0.476	2	0.010	0.375	12248
J1210−2758	0.828	STIS	G230L	0	—	—	1	—	—	8225
J1211+3657	0.170	COS	G130M-G160M	1	0.010	0.270	2	0.010	0.159	12248
J1211+1030	2.193	FOS	G160L	0	—	—	0	—	—	5351
J1214+1403	0.085	FOS	G130H-G270H-G190H	1	0.010	0.184	0	—	—	1026
J1214+0825	0.585	COS	G130M	1	0.010	0.186	2	0.010	0.186	11698
J1214+1429	1.626	STIS	G230L	0	—	—	1	—	—	7359
J1216+0712	0.586	COS	G130M	1	0.010	0.183	2	0.010	0.183	11698
J1216+1747	0.375	FOS	G190H	1	0.356	0.474	1	0.356	0.361	5456
J1217+0809	0.342	COS	G130M	1	0.010	0.183	2	0.010	0.183	11698
J1217+6407	1.288	FOS	G270H	1	0.914	1.387	1	0.914	1.265	5441
J1218+1105	1.403	FOS	G160L	1	0.625	1.065	1	0.625	1.065	2424
J1218+5015	1.450	FOS	G270H	1	0.829	1.549	1	0.829	1.425	6432
J1218+1015	0.542	COS	G130M	1	0.010	0.187	2	0.010	0.187	11698
J1219+0638	0.331	COS	G130M-G160M	1	0.010	0.431	1	0.010	0.318	12025
		FOS	G270H-G190H-G130H	1	—	—	1	—	—	3791,4112
J1220+0641	0.286	COS	G130M	1	0.010	0.183	2	0.010	0.183	11698
J1220−2113	0.800	STIS	G230L	1	0.526	0.899	1	0.526	0.782	8225
J1220+3343	1.532	STIS	G230L	1	0.288	1.589	0	—	—	8569
J1220+3853	0.375	COS	G130M-G160M	1	0.010	0.475	2	0.010	0.361	11598
J1220−0040	1.411	STIS	G230L	1	0.556	1.510	0	—	—	9382
J1221+1554	0.229	COS	G130M	1	0.010	0.183	2	0.010	0.183	11698
J1221+4548	0.525	COS	G130M	1	0.106	0.210	2	0.106	0.210	12486
J1221+0430	0.094	FOS	G270H-G130H	1	0.010	0.193	2	0.010	0.083	5451
J1221+7518	0.070	FOS	G270H-G190H-G130H	1	0.010	0.169	1	0.010	0.059	1022,4952
J1223+0950	0.277	COS	G130M	1	0.010	0.183	2	0.010	0.183	11698
J1223+0923	0.681	COS	G130M	1	0.010	0.187	2	0.010	0.187	11698
J1223+1545	0.081	FOS	G130H-G270H	1	—	—	1	—	—	4952,5451
J1224+0037	1.482	STIS	G230L	1	0.742	1.581	0	—	—	9382
J1225−2938	0.816	STIS	G230L	1	0.412	0.915	1	0.412	0.797	8225
J1225+1218	0.411	COS	G130M	1	0.010	0.183	2	0.010	0.183	11698
J1225+0844	0.535	COS	G130M	1	0.010	0.183	2	0.010	0.183	11698
J1225+2235	2.046	FOS	G190H-G270H	1	0.679	0.901	1	0.679	0.901	2524,6577
J1225+3332	0.001	COS	G130M-G160M	1	0.010	0.101	1	—	—	12212
J1225+0035	1.226	STIS	G230L	1	0.637	1.325	0	—	—	9382
J1225−0052	0.964	STIS	G230L	2	—	—	0	—	—	9382
J1226−0006	1.118	STIS	G230L	1	0.709	1.217	0	—	—	9382
J1226−2630	0.768	STIS	G230L	1	0.753	0.867	1	—	—	8225
J1228+3128	2.219	FOS	G270H	1	1.107	1.696	1	1.107	1.696	5095
J1228+1018	2.304	STIS	G230L	1	1.050	1.597	0	—	—	8569
J1229+0203	0.173	COS	G130M	1	0.010	0.209	1	0.010	0.161	12038
J1230+0115	0.117	COS	G130M-G160M	1	0.010	0.216	1	0.010	0.105	11686
J1232−0224	1.045	COS	G160M	1	0.159	0.462	0	—	—	12593
		FOS	G190H-G270H	1	0.463	1.144	0	—	—	1193,3939,5351
		FOS	G160L	1	—	—	0	—	—	1193,3939
J1232+2009	0.063	COS	G130M	1	0.010	0.163	1	0.010	0.052	12569
J1232+5252	4.294	STIS	G140L	0	—	—	0	—	—	9759
J1233−0031	0.471	COS	G130M-G160M	1	0.010	0.476	2	0.010	0.456	12486
J1233+0931	0.420	FOS	G130H-G190H	1	0.362	0.519	1	0.362	0.405	4952
J1233+4758	0.381	COS	G130M-G160M	1	0.010	0.430	2	0.010	0.368	13033
J1234+0724	0.843	COS	G130M	1	0.010	0.183	2	0.010	0.183	11698
J1235+4736	4.447	STIS	G140L	0	—	—	1	—	—	8582
J1236+2641	0.209	COS	G130M-G160M	1	0.010	0.308	2	0.010	0.196	12248
J1236+0600	1.279	COS	G130M	1	0.061	0.186	2	0.061	0.186	11698
J1238+1750	0.449	STIS	G230L	2	—	—	1	—	—	7359
J1240+0949	1.045	COS	G130M	1	0.062	0.187	2	0.062	0.187	11698

Table 1 — *Continued*

QSO	z_{em} [a]	Instrument	Grating	Search Path			Statistical Path			Proposal ID
				F_{search} [b]	Min z	Max z	F_{stat} [c]	Min z	Max z	
J1241+2852	0.590	COS	G130M	1	0.010	0.207	2	0.010	0.207	12603
J1241+5721	0.583	COS	G130M-G160M	1	0.010	0.430	2	0.010	0.430	11598
J1242+0012	1.213	STIS	G230L	1	0.507	1.313	1	0.507	1.191	7359
J1244+1721a	1.283	FOS	G270H	1	0.829	1.382	1	0.829	1.260	4112
J1244+1721b	1.283	COS	G160M	1	0.169	0.462	0	—	—	12466
J1245+3356	0.717	COS	G130M-G160M	1	0.010	0.476	2	0.010	0.476	11598
J1246−0730	1.286	STIS	G230L	1	0.918	1.385	0	—	—	9076
J1247+3126	2.960	STIS	G140L	0	—	—	1	—	—	8287
J1249−0559	2.226	STIS	G140L	0	—	—	1	—	—	7295,4081
J1250+2631	2.043	FOS	G270H	1	0.829	1.695	1	0.829	1.695	5095,6705
J1250−2333	0.048	COS	G130M	1	0.010	0.147	2	0.010	0.037	13027
J1250+3016	1.061	FOS	G270H-G190H	1	0.990	1.160	1	0.990	1.040	5441
J1250+3951	1.030	FOS	G190H-G270H	1	0.351	1.129	1	0.351	1.009	5664
J1251+0554	1.377	COS	G130M	1	0.010	0.210	2	0.010	0.210	12603
J1251+4637	1.460	COS	G160M	1	0.158	0.462	0	—	—	12593
J1252+2913	0.820	FOS	G190H	1	0.337	0.901	1	0.337	0.801	6007
J1252+5634	0.321	FOS	G190H-G270H	1	—	—	1	—	—	2578
J1253+3106	0.780	FOS	G190H	1	0.332	0.879	1	0.332	0.762	6007
J1254+1141	0.870	FOS	G190H-G270H	1	0.363	0.969	1	0.363	0.851	2424
		FOS	G160L	1	—	—	1	—	—	2424
J1256−0547	0.538	FOS	G190H-G270H-G130H	1	0.060	0.637	1	0.060	0.522	2578,5936
J1256+5652	0.041	COS	G130M	1	0.010	0.141	1	0.010	0.031	12569
J1259+3423	1.375	FOS	G270H	1	0.835	1.474	1	0.835	1.351	5225
J1301+2819	1.355	FOS	G270H	1	0.830	1.454	2	0.830	1.331	5501
J1301+5902	0.472	COS	G130M-G160M	1	0.010	0.476	1	0.010	0.457	11541
		FOS	G190H-G270H-G130H	1	0.477	0.571	1	—	—	2424,3418
		STIS	G140L	1	—	—	2	—	—	7295
J1304−0037	3.035	STIS	G140L	0	—	—	1	—	—	9067
J1305+0357	0.545	COS	G130M	1	0.010	0.210	2	0.010	0.210	12603
J1305−1033	0.278	COS	G130M-G160M	1	0.010	0.378	1	0.010	0.265	12038
		FOS	G190H-G270H-G130H	1	—	—	1	—	—	3222,3791,5664
J1307+0641	0.602	FOS	G190H-G270H	1	0.366	0.701	1	0.366	0.586	5441
J1308+3005	0.806	FOS	G270H	1	—	—	1	—	—	4952
		FOS	G160L	1	0.173	0.905	1	0.173	0.788	4952
J1309+0819	0.154	COS	G130M	1	0.010	0.208	1	0.010	0.142	12569
		FOS	G190H	1	—	—	1	—	—	4953
J1310+4601	2.129	FOS	G270H-G190H	1	0.335	1.697	1	0.335	1.697	5950
J1312+3515	0.184	COS	G130M	1	0.010	0.194	1	0.010	0.172	12569
		FOS	G270H-G190H-G130H	1	0.195	0.283	1	—	—	6781
J1313−2716	2.186	STIS	G230L	1	1.024	1.591	0	—	—	8569
J1314+0201	0.306	FOS	G190H	1	—	—	1	—	—	5456
J1314−3105	0.000	STIS	G140L	0	—	—	1	—	—	8287
J1315+1525	0.449	COS	G130M	1	0.010	0.207	2	0.010	0.207	12603
J1317+3531	4.360	STIS	G140L	0	—	—	1	—	—	8582
J1318+2628	1.234	COS	G130M	1	0.010	0.210	2	0.010	0.210	12603
J1319+5147	1.055	FOS	G270H	1	0.834	1.154	1	0.834	1.034	4953
		FOS	G160L	1	0.471	0.833	1	0.471	0.833	4953
J1319−0158	0.225	FOS	G190H	1	—	—	1	—	—	5456
J1319+2728	1.022	COS	G160M	1	0.253	0.461	2	0.253	0.461	11667
		FOS	G190H-G270H	1	0.462	1.121	1	0.462	1.001	2424
		FOS	G160L	1	0.252	0.252	1	0.252	0.252	2424
J1321+2847a	1.703	FOS	G190H	1	0.611	0.901	1	0.611	0.901	1144,6007
		FOS	G160L	1	0.902	1.065	1	0.902	1.065	1144
J1321+2847b	0.549	FOS	G270H-G190H	1	0.352	0.648	1	0.352	0.533	1144,6007
J1321+1106	2.181	STIS	G230L	1	—	—	0	—	—	8569
J1322+4645	0.375	COS	G130M-G160M	1	0.010	0.430	2	0.010	0.361	13033
J1322+4739	1.101	STIS	G230L	1	0.474	1.201	1	0.474	1.080	8126
J1323+2910	0.966	FOS	G270H-G190H	1	0.411	1.065	1	0.411	0.946	4953,6007
		FOS	G160L	1	—	—	1	—	—	4953
J1323−0021	1.388	STIS	G230L	1	0.840	1.487	0	—	—	9382
J1323+3430	0.444	COS	G160M	1	0.152	0.450	0	—	—	12593
J1323+6541	0.168	FOS	G130H-G270H-G190H	1	0.010	0.267	1	0.010	0.156	6781
J1324+0537	0.205	FOS	G190H	1	—	—	1	—	—	6799
J1324+0446	0.021	COS	G160M	0	—	—	1	—	—	12557
J1325+2717	0.522	COS	G130M	1	0.010	0.210	2	0.010	0.210	12603
J1325+6515	1.618	FOS	G270H	1	0.975	1.697	0	—	—	6577
J1327+4435	0.330	COS	G130M-G160M	1	0.010	0.430	2	0.010	0.317	12248
J1328+5244	1.341	COS	G160M	1	0.162	0.459	0	—	—	12593
J1330−2056	1.169	FOS	G270H	1	0.830	1.268	1	0.830	1.147	5654
		STIS	G140L	1	—	—	0	—	—	9382
J1330+2813	0.416	COS	G130M-G160M	1	0.010	0.476	2	0.010	0.402	11598
J1330+3119	0.242	COS	G130M-G160M	1	0.010	0.342	2	0.010	0.229	12248
J1331+3030	0.849	FOS	G190H-G270H	1	0.343	0.948	0	—	—	1193,5351
		FOS	G160L	1	0.113	0.342	0	—	—	1193
J1331+4101	1.930	FOS	G190H-G270H	1	0.739	1.696	0	—	—	5948,6577

Table 1 — *Continued*

QSO	z_{em} [a]	Instrument	Grating	Search Path			Statistical Path			Proposal ID
				F_{search} [b]	Min z	Max z	F_{stat} [c]	Min z	Max z	
J1333+2539	3.030	STIS	G140L	0	—	—	1	—	—	8287
J1336+1725	0.554	FOS	G190H-G270H	1	0.353	0.653	1	0.353	0.538	2424
		FOS	G160L	1	—	—	1	—	—	2424
J1336−0048	2.801	FOS	G160L	1	0.763	1.065	1	0.763	1.065	3268
J1336−0049	2.783	FOS	G270H-G190H-G130H	1	0.353	1.696	1	0.353	1.696	5492
J1337+2422	0.108	FOS	G190H-G270H	1	—	—	1	—	—	5928
J1341+4123	1.219	COS	G130M-G160M	1	0.010	0.480	1	0.010	0.480	11741
		FOS	G270H-G190H	1	0.481	1.318	1	0.481	1.196	2424,3837,6612
		FOS	G160L	1	—	—	1	—	—	2424
J1341+0059	1.714	STIS	G230L	1	0.288	1.589	0	—	—	9382
J1342+0505	0.266	COS	G130M-G160M	1	0.010	0.366	2	0.010	0.253	12248
J1342+6021	0.960	FOS	G270H	1	0.834	1.060	1	0.834	0.941	3858
		STIS	G230L	1	0.010	0.833	1	0.010	0.833	7356
J1342+3829	0.171	COS	G130M-G160M	1	0.010	0.271	2	0.010	0.160	12248
J1342−0035	0.786	STIS	G230L	1	0.288	0.886	0	—	—	9382
J1342+1844	0.382	COS	G130M-G160M	1	0.010	0.476	2	0.010	0.368	12248
J1342−0054	0.326	FOS	G190H	1	0.348	0.425	1	—	—	5456
J1342−0053	0.325	COS	G130M-G160M	1	0.010	0.425	2	0.010	0.312	11598
J1343+2844	0.905	FOS	G160L	1	0.578	1.004	1	0.578	0.886	2424
J1345−0023	1.094	STIS	G230L	1	0.559	1.194	0	—	—	9382
J1348+2818	2.941	STIS	G140L	0	—	—	1	—	—	8287
J1348+2456	0.293	COS	G130M	1	0.010	0.206	2	0.010	0.206	12603
J1348+2622	0.598	FOS	G270H	1	—	—	2	—	—	6548
J1351−0007	1.444	FOS	G160L	1	0.641	1.065	1	0.641	1.065	4953
J1352−2649	0.934	STIS	G230L	1	0.896	1.033	1	0.896	0.914	8225
J1353+6918	0.030	COS	G130M-G160M	1	0.010	0.130	1	0.010	0.020	12212
J1353+6345	0.088	COS	G130M	1	0.010	0.187	1	0.010	0.077	12569
		FOS	G130H-G270H-G190H	1	—	—	2	—	—	2717
J1354+3138	1.326	FOS	G270H	1	0.856	1.425	1	0.856	1.302	5441
J1354+2430	1.878	COS	G130M	1	0.010	0.207	2	0.010	0.207	12603
J1354+1805	0.152	FOS	G270H-G190H-G130H	1	0.019	0.251	1	0.019	0.140	6781
J1354+0052	1.117	FOS	G190H-G270H	1	0.342	1.216	1	0.342	1.095	2424,6612
		FOS	G160L	1	0.114	0.341	1	0.114	0.341	2424
J1356+2515	0.164	COS	G130M-G160M	1	0.010	0.264	2	0.010	0.152	12248
J1357+1919	0.719	COS	G160M	1	0.139	0.442	2	0.139	0.442	13398
		FOS	G190H-G270H	1	0.443	0.819	1	0.443	0.702	2424,3858
		FOS	G160L	1	—	—	1	—	—	2424
J1357+1704	0.150	COS	G130M-G160M	1	0.010	0.250	2	0.010	0.139	12248
J1357+0435	1.231	COS	G130M-G160M	1	0.010	0.480	2	0.010	0.480	12264
J1358+5752	1.375	FOS	G270H	1	0.844	1.474	1	0.844	1.351	4504
J1358−2352	0.831	STIS	G230L	1	0.498	0.931	1	0.498	0.813	8225
J1359−4152	0.313	FOS	G190H	1	—	—	1	—	—	4953
J1359+5726	0.033	COS	G130M	1	0.010	0.133	2	0.010	0.023	12583
J1400+5535	0.840	COS	G160M	1	0.162	0.459	0	—	—	12593
J1402−2822	0.802	STIS	G230L	1	0.528	0.902	1	0.528	0.784	8225
J1404+0937	0.441	FOS	G190H	1	0.407	0.540	1	0.407	0.426	4953
J1404+3353	0.549	COS	G130M	1	0.010	0.207	2	0.010	0.207	12603
J1404−0130	2.522	STIS	G230L	1	1.059	1.612	0	—	—	8569
J1405+2555	0.164	FOS	G190H-G130H-G270H	1	0.010	0.263	1	0.010	0.152	4953,5456,6781
J1406+2223	0.098	FOS	G270H-G190H-G130H	1	0.010	0.197	1	0.010	0.087	6247
J1406+0157	0.426	COS	G130M	1	0.010	0.210	2	0.010	0.210	12603
J1407+5507	1.027	COS	G130M	1	0.010	0.210	2	0.010	0.210	12486
J1409+2618	0.945	COS	G130M-G160M	1	0.010	0.480	1	0.010	0.480	11741
		FOS	G190H-G270H	1	0.481	1.044	1	0.481	0.925	2424
		FOS	G160L	1	—	—	1	—	—	2424
J1410+2955	0.570	COS	G160M	0	—	—	0	—	—	12593
J1410+2304	0.795	COS	G130M-G160M	1	0.010	0.472	2	0.010	0.472	12958
J1413+4400	0.090	COS	G130M	1	0.010	0.189	1	0.010	0.079	12569
J1415+1634	0.743	COS	G130M	1	0.010	0.193	2	0.010	0.193	12486
J1417+4456	0.114	FOS	G270H-G190H-G130H	1	0.010	0.213	1	0.010	0.102	3566,6781
J1417+4330	0.002	COS	G130M	1	0.010	0.102	1	—	—	11579
		FOS	G190H	1	—	—	1	—	—	5408
J1417+2508	0.016	COS	G130M-G160M	1	0.010	0.116	1	—	—	12212
J1418+1703	0.821	FOS	G160L	1	0.524	0.920	1	0.524	0.802	2424
J1419−1310	0.129	FOS	G190H	1	—	—	1	—	—	6528
J1419+0628	1.436	FOS	G270H	1	0.830	1.535	1	0.830	1.411	6589
J1419+4207	0.873	COS	G130M-G160M	1	0.010	0.476	2	0.010	0.476	11598
J1419−0036	0.969	STIS	G230L	1	0.469	1.068	0	—	—	9382
J1420−0054	1.458	STIS	G230L	1	0.781	1.557	0	—	—	9382
J1421+2538	1.050	COS	G160M	1	0.142	0.440	0	—	—	12593
J1423+3252	1.904	STIS	G230L	1	0.872	1.612	0	—	—	8569
J1426+0051	1.333	STIS	G230L	1	0.485	1.432	0	—	—	9382
J1427+2348	0.160	COS	G130M-G160M	1	0.010	0.259	1	0.010	0.148	12612
J1427+1949	0.111	FOS	G190H	1	—	—	1	—	—	4953
J1427+2632	0.366	COS	G130M	1	0.010	0.205	2	0.010	0.205	12603

Table 1 — *Continued*

QSO	z_{em} [a]	Instrument	Grating	Search Path			Statistical Path			Proposal ID
				F_{search} [b]	Min z	Max z	F_{stat} [c]	Min z	Max z	
		FOS	G270H-G190H	1	0.297	0.465	1	0.297	0.352	6781
J1427−1203	0.805	FOS	G190H-G270H	1	0.381	0.904	1	0.381	0.787	2424
		FOS	G160L	1	—	—	1	—	—	2424
J1429+0321	0.253	COS	G130M	1	0.010	0.207	2	0.010	0.207	12603
J1429+4747	0.221	FOS	G130H-G270H-G190H	1	0.010	0.320	1	0.010	0.208	6781
J1430+0222	0.353	COS	G130M	1	0.053	0.179	2	0.053	0.179	12539
J1431+3952	1.215	STIS	G230L	1	0.383	1.315	0	—	—	9051
J1431+2442	0.406	COS	G130M	1	0.010	0.210	2	0.010	0.210	12603
J1431−0050	1.188	STIS	G230L	1	0.618	1.288	0	—	—	9382
J1435+3604	0.428	COS	G130M-G160M	1	0.010	0.476	2	0.010	0.414	11598
J1436+5847	0.031	COS	G130M-G160M	1	0.010	0.130	1	0.010	0.020	11505
J1436−0051	1.273	STIS	G230L	1	0.681	1.372	0	—	—	9382
J1436+6336	2.068	FOS	G270H	1	1.201	1.695	1	1.201	1.695	3221
J1436+4952	1.550	STIS	G230L	2	—	—	1	—	—	7359
J1437+5045	0.783	COS	G130M-G160M	1	0.010	0.476	2	0.010	0.476	11598
J1437−0147	1.310	COS	G130M-G160M	1	0.010	0.480	1	0.010	0.480	11741
		FOS	G270H	1	0.832	1.409	1	0.832	1.286	4953,6103
		FOS	G160L	1	0.803	0.831	1	0.803	0.831	6103,4953
J1438−0658	0.129	COS	G130M	1	0.010	0.192	1	0.010	0.117	12569
		STIS	G230L	1	—	—	1	—	—	9507
J1438+6211	1.090	STIS	G230L	1	0.291	1.189	0	—	—	8569
J1439+2954	2.990	STIS	G140L	0	—	—	1	—	—	8287
J1442+3526	0.077	COS	G130M	1	0.010	0.176	1	0.010	0.066	12569
		FOS	G190H-G270H-G130H	1	—	—	1	—	—	4953,6781
J1445+3428	0.697	COS	G130M-G160M	1	0.010	0.476	2	0.010	0.476	11598
J1446+4035	0.267	FOS	G270H-G190H-G130H	1	0.010	0.366	1	0.010	0.254	3566,6781
J1451+2709	0.064	COS	G130M-G160M	1	0.010	0.164	2	0.010	0.053	12248
J1454+3046	0.465	COS	G130M	1	0.010	0.210	2	0.010	0.210	12603
J1454−3747	0.314	FOS	G190H-G130H	1	0.297	0.413	0	—	—	4342,5948
J1455−0045	1.374	STIS	G230L	1	0.604	1.474	0	—	—	9382
J1459+7140	0.904	COS	G130M	1	0.010	0.210	2	0.010	0.210	12486
J1459+5319	0.338	COS	G130M	1	0.010	0.206	2	0.010	0.206	12276
J1500+5517	0.404	COS	G130M	1	0.010	0.206	2	0.010	0.206	12276
J1501+0019	1.930	STIS	G230L	1	0.288	1.589	0	—	—	9382
J1502+0645	0.287	COS	G130M	1	0.010	0.210	2	0.010	0.210	12603
J1502−4154	1.026	COS	G130M	1	0.072	0.210	1	0.072	0.210	11659
		STIS	G230L	1	0.620	1.125	1	0.620	1.005	8244
J1503+6105	3.682	STIS	G140L	0	—	—	0	—	—	9759
J1503+6810	0.114	COS	G130M	1	0.010	0.206	2	0.010	0.102	12276
J1503−4152	0.335	COS	G130M	1	0.010	0.211	1	0.010	0.211	11659
		STIS	G230L	1	0.212	0.434	1	0.212	0.321	8244
J1504+6856	0.318	FOS	G270H	1	—	—	2	—	—	6719
J1504+0122	0.967	STIS	G140L	1	0.020	0.412	2	0.020	0.412	9874
J1504+5649	0.358	COS	G130M	1	0.010	0.206	2	0.010	0.206	12276
J1505+0342	0.036	STIS	G140L	1	0.010	0.136	2	0.010	0.025	9874
J1508+6717	0.716	STIS	G140L	1	—	—	2	—	—	7762
J1508+6814	0.058	COS	G130M	1	0.010	0.158	2	0.010	0.047	12276
J1509+0702	0.417	COS	G130M	1	0.010	0.210	2	0.010	0.210	12603
J1509+1110	0.285	COS	G130M	1	0.010	0.179	0	—	—	12614
J1510+0058	0.070	STIS	G140L	1	0.010	0.169	2	0.010	0.059	9874
J1512+0128	0.265	COS	G130M	1	0.010	0.210	2	0.010	0.210	12603
J1513+1011	1.546	FOS	G160L	1	0.113	0.994	0	—	—	6577
J1514+3619	0.695	COS	G130M-G160M	1	0.065	0.477	2	0.065	0.477	11598
J1514+3650	0.371	FOS	G190H-G270H	1	0.334	0.470	1	0.334	0.357	2424,3538
J1515+0657	0.267	COS	G130M	1	0.010	0.207	2	0.010	0.207	12603
J1516+1900	0.190	STIS	G230L	1	0.010	0.289	1	0.010	0.178	9161
J1519+2346a	1.834	FOS	G190H-G270H	1	0.370	1.696	1	0.370	1.696	5320,5631
J1519+2346b	1.903	FOS	G190H-G270H	1	0.490	1.695	1	0.490	1.695	5320
J1519+5908	0.078	COS	G130M	1	0.010	0.178	2	0.010	0.067	12276
J1521−0009	1.318	STIS	G230L	1	0.676	1.417	0	—	—	9382
J1521+0337	0.126	COS	G130M-G160M	1	0.010	0.226	2	0.010	0.115	12248
J1521+5940	0.286	COS	G130M	1	0.010	0.206	2	0.010	0.206	12276
J1523+6339	0.204	COS	G130M	1	0.010	0.207	2	0.010	0.192	12276
J1524+0958	1.324	COS	G130M-G160M	1	0.010	0.480	1	0.010	0.480	11741
		FOS	G270H-G190H	1	0.481	1.423	0	—	—	3200,6705
		FOS	G160L	1	—	—	0	—	—	3200
J1525+0026	0.801	STIS	G230L	1	0.422	0.900	0	—	—	9382
J1527+2452	0.993	STIS	G230L	1	0.576	1.092	0	—	—	9051
J1527+6548	0.345	COS	G130M	1	0.010	0.206	2	0.010	0.206	12276
J1528+2825	0.450	COS	G130M-G160M	1	0.010	0.476	1	0.010	0.435	12038
J1529+5616	0.099	COS	G130M	1	0.010	0.199	2	0.010	0.088	12276
J1535+5754	0.030	COS	G130M-G160M	1	0.010	0.130	1	0.010	0.019	11524
J1536+5433	0.039	COS	G130M	1	0.010	0.138	2	0.010	0.028	12276
J1537+0021	1.754	STIS	G230L	1	1.018	1.589	0	—	—	9382
J1537+3358	1.025	STIS	G230L	1	0.463	1.124	0	—	—	9051

Table 1 — *Continued*

QSO	z_{em} [a]	Instrument	Grating	Search Path			Statistical Path			Proposal ID
				F_{search} [b]	Min z	Max z	F_{stat} [c]	Min z	Max z	
J1538+5736	0.073	COS	G130M	1	0.010	0.173	2	0.010	0.062	12276
J1539+4735	0.770	FOS	G270H-G190H	1	0.341	0.869	1	0.341	0.752	3791,4118
		FOS	G160L	1	0.331	0.340	1	0.331	0.340	3791
J1541+2817	0.375	COS	G130M	1	0.010	0.206	2	0.010	0.206	12603
J1544+5358	2.371	FOS	G270H-G130H-G190H	1	0.527	1.696	1	0.527	1.696	6293
J1544+5912	0.807	STIS	G230L	1	0.010	0.906	2	0.010	0.789	8485
J1544+2743	0.163	COS	G130M	1	0.010	0.206	2	0.010	0.151	12603
J1545+4846	0.400	FOS	G130H-G190H	1	0.010	0.499	1	0.010	0.386	4953,5451
J1545+0936	0.664	COS	G130M-G160M	1	0.111	0.457	2	0.111	0.457	12248
J1547+2052	0.264	COS	G130M-G160M	1	0.010	0.363	2	0.010	0.251	13398
		FOS	G130H-G190H-G270H	1	—	—	1	—	—	2578
J1550+4001	0.496	COS	G130M-G160M	1	0.010	0.476	2	0.010	0.476	11598
J1552+5705	0.366	COS	G130M	1	0.010	0.206	2	0.010	0.206	12276
J1553+3548	0.722	COS	G130M-G160M	1	0.010	0.476	2	0.010	0.476	11598
J1554+0822	0.119	STIS	G230L	1	—	—	1	—	—	9507
J1555+3628	0.713	COS	G130M-G160M	1	0.010	0.476	2	0.010	0.476	11598
J1555+1111	0.360	COS	G130M-G160M	1	0.010	0.459	1	0.010	0.346	12025
J1557−2029	1.947	STIS	G230L	1	1.211	1.609	0	—	—	8569
J1557+3304	0.942	FOS	G270H	1	0.902	1.041	1	0.902	0.922	3858
J1559−2442	2.818	STIS	G230L	0	—	—	0	—	—	8569
J1601+1714	1.952	FOS	G160L	1	0.944	1.065	1	0.944	1.065	5095
J1603+5730	2.850	COS	G130M	1	0.010	0.124	0	—	—	12816
J1605+1448	0.371	COS	G130M	1	0.010	0.179	0	—	—	12614
J1608+6018	0.178	COS	G130M	1	0.010	0.207	2	0.010	0.166	12276
J1613+3412	1.401	FOS	G270H	1	0.857	1.500	1	0.857	1.377	2578
J1613+6543	0.138	COS	G130M-G160M	1	0.010	0.238	1	0.010	0.127	11686
J1614+2604	0.131	FOS	G190H	1	—	—	1	—	—	4953
J1614+4859	3.799	STIS	G140L	0	—	—	0	—	—	9759
J1614+4704	1.859	STIS	G230L	1	0.826	1.611	0	—	—	9051
J1616+4154	0.440	COS	G130M-G160M	1	0.010	0.476	2	0.010	0.426	11598
J1617+0638	0.229	COS	G130M-G160M	1	0.010	0.329	2	0.010	0.216	11598
J1619+3342	0.470	COS	G130M-G160M	1	0.010	0.476	2	0.010	0.456	11598
J1619+3813	1.124	STIS	G140L	1	0.010	0.412	2	0.010	0.412	9874
J1620+1724	0.112	COS	G130M	1	0.010	0.193	1	0.010	0.100	12569
J1620+1736	0.555	FOS	G190H-G270H	1	0.344	0.654	1	0.344	0.539	2424,2578
		FOS	G160L	1	0.310	0.343	1	0.310	0.343	2424
J1624+2345	0.927	FOS	G270H-G190H	1	0.454	1.026	0	—	—	5304
J1625+5727	0.067	COS	G130M	1	0.010	0.166	2	0.010	0.056	12276
J1625+2646	2.526	FOS	G270H	1	0.830	1.695	0	—	—	6577
		FOS	G160L	1	0.540	0.829	0	—	—	6577
J1627+5522	0.133	COS	G130M-G160M	1	0.010	0.232	1	0.010	0.121	12029
		FOS	G130H-G270H-G190H	1	—	—	1	—	—	6781
J1630+3758	1.461	FOS	G160L	1	0.588	1.065	1	0.588	1.065	1144
J1631+4048	0.257	STIS	G140L	1	0.010	0.357	1	0.010	0.244	9506
J1631+1156	1.792	STIS	G230L	1	0.727	1.605	0	—	—	8569
J1632+3737	1.478	COS	G130M-G160M	1	0.010	0.480	1	0.010	0.480	11741
		FOS	G190H-G270H	1	0.481	1.577	1	0.481	1.453	3837,5698
J1633+3924	1.023	FOS	G270H	1	0.940	1.122	1	0.940	1.002	4953
J1634+7031	1.337	FOS	G270H-G190H	1	0.830	1.436	1	0.830	1.313	3221,3732
J1636+7205	0.187	STIS	G140L	1	0.019	0.286	1	0.019	0.175	9506
J1637+2509	1.110	STIS	G230L	1	0.549	1.209	0	—	—	9051
J1638+5720	0.745	FOS	G190H-G270H	1	0.367	0.844	1	0.367	0.727	4052
J1642+3924	2.383	COS	G130M-G160M	0	—	—	2	—	—	13398
J1642+3948	0.595	FOS	G190H-G270H	1	0.449	0.694	1	0.449	0.579	2578,6214
J1649+3047	1.350	STIS	G230L	0	—	—	1	—	—	8266
J1649+3046	1.122	STIS	G230L	1	0.567	1.222	1	0.567	1.101	8266
J1658+0515	0.879	FOS	G270H	1	0.883	0.978	1	—	—	2424,5441
		FOS	G160L	1	0.881	0.882	1	—	—	2424
J1659+3735	0.771	COS	G160M	1	0.162	0.459	0	—	—	12593
J1701+6411	2.722	FOS	G130H-G190H-G270H	1	0.354	1.695	1	0.354	1.695	2288,6433
		STIS	G230L	1	0.010	0.353	1	0.010	0.353	9982
J1701+2924	0.036	COS	G130M	1	0.010	0.136	1	0.010	0.025	12275
J1702+6058	0.164	STIS	G230L	1	0.011	0.263	2	0.011	0.152	8024
J1703+6141	0.077	COS	G130M	1	0.010	0.177	2	0.010	0.066	12276
J1703+5813	0.106	COS	G130M	0	—	—	2	—	—	12533
J1704+7057	2.015	STIS	G230L	1	1.115	1.606	0	—	—	8569
J1704+6044	0.371	FOS	G130H-G190H-G270H	1	0.010	0.470	1	0.010	0.357	2424,3418
J1706+3615	0.918	STIS	G230L	1	0.405	1.017	0	—	—	9051
J1710+5923	4.470	STIS	G230L	0	—	—	0	—	—	9759
J1711+6052	3.835	STIS	G140L	0	—	—	0	—	—	9759
J1712+5559	1.358	STIS	G230L	1	0.685	1.457	0	—	—	9382
J1714+5757	1.252	STIS	G230L	2	—	—	0	—	—	9382
J1715+6453	3.960	STIS	G140L	0	—	—	0	—	—	9759
J1715+4606	0.985	STIS	G230L	1	0.671	1.084	0	—	—	9051
J1715+5747	0.697	STIS	G230L	1	0.423	0.796	0	—	—	9382

Table 1 — *Continued*

QSO	z_{em} [a]	Instrument	Grating	Search Path			Statistical Path			Proposal ID
				F_{search} [b]	Min z	Max z	F_{stat} [c]	Min z	Max z	
J1716+5654	0.937	STIS	G230L	1	0.554	1.036	0	—	—	9382
J1716+5328	1.940	FOS	G270H	1	0.834	1.696	1	0.834	1.696	5664
		FOS	G160L	1	—	—	0	—	—	6577
J1717+6559	0.292	COS	G130M	1	0.010	0.206	2	0.010	0.206	12276
J1717+5500	0.211	STIS	G140L	0	—	—	1	—	—	9067
J1719+4858	0.025	FOS	G270H-G190H-G130H	1	—	—	1	—	—	5428
J1719+4804	1.084	FOS	G270H-G190H	1	0.343	1.183	1	0.343	1.063	4112,4817,6705
J1722+5442	1.215	STIS	G230L	1	0.650	1.314	0	—	—	9382
J1727+5302	1.444	STIS	G230L	1	0.666	1.543	0	—	—	9382
J1728−1415	0.184	STIS	G230L	1	0.010	0.283	1	0.010	0.172	8264
J1729+7032	0.533	STIS	G140L	0	—	—	1	—	—	9506
J1729+5758	1.342	STIS	G230L	1	0.549	1.441	0	—	—	9382
J1733+5533	1.072	STIS	G230L	1	0.518	1.171	0	—	—	9382
J1734+6702	0.026	COS	G130M	0	—	—	2	—	—	12276
J1736+5938	1.410	STIS	G230L	1	0.818	1.509	0	—	—	9382
J1742+1827	0.186	STIS	G230L	1	0.010	0.285	1	0.010	0.174	8684
J1800+7828	0.680	FOS	G190H-G270H	1	0.384	0.779	1	0.384	0.663	5441
J1821+6420	0.297	COS	G130M	1	0.010	0.209	1	0.010	0.209	12038
J1822+6420	0.297	FOS	G190H-G270H-G130H	1	0.010	0.396	1	0.010	0.284	1025,3221
J1824+1044	1.360	FOS	G190H	1	0.750	0.901	0	—	—	6577
J1825−1358	0.000	COS	G130M-G160M	1	0.010	0.099	1	—	—	12023
J1832+5340	0.039	COS	G130M	1	0.010	0.138	1	0.010	0.028	12275
J1842+7946	0.056	FOS	G270H-G130H-G190H	1	0.010	0.155	1	0.010	0.045	6097
J1858+5645	1.595	STIS	G230L	1	0.695	1.604	0	—	—	8569
J1902+3159	0.635	FOS	G160L	1	0.246	0.734	0	—	—	6577
J1921−5840	0.036	COS	G130M-G160M	1	0.010	0.136	1	0.010	0.026	12936
J1927+7358	0.302	FOS	G270H-G190H	1	0.010	0.401	1	0.010	0.289	4112,5441
J1939+7007	0.120	STIS	G140L	1	0.010	0.219	1	0.010	0.108	9506
J1940−6907	3.152	STIS	G140L	0	—	—	1	—	—	7272
J1944+7705	3.051	STIS	G140L	0	—	—	1	—	—	8582
J2006−0223	1.457	STIS	G230L	0	—	—	0	—	—	8569
J2009−4849	0.071	COS	G130M-G160M	1	0.010	0.171	1	0.010	0.060	11520
J2044−1043	0.035	COS	G130M-G160M	1	0.010	0.134	1	0.010	0.024	12916
		FOS	G130H-G190H-G270H	1	—	—	1	—	—	4045
J2051+1950	2.367	STIS	G230L	1	1.170	1.608	0	—	—	8569
J2114+0607	0.457	STIS	G230L	1	0.010	0.556	1	0.010	0.442	9277
J2115−4323	1.708	STIS	G230L	2	—	—	1	—	—	7359
J2115+0608	0.453	FOS	G190H-G270H	1	0.351	0.552	1	0.351	0.438	4112
J2120−4426	1.480	STIS	G230L	1	0.622	1.579	1	0.622	1.455	7359
J2131−1207	0.501	COS	G130M-G160M	1	0.053	0.480	2	0.053	0.480	13398
		FOS	G190H-G270H	1	0.481	0.600	1	0.481	0.486	4581
J2132+1008	0.061	COS	G130M-G160M	1	0.010	0.161	1	0.010	0.051	11524
J2136−6224	0.058	COS	G130M-G160M	1	0.010	0.158	1	0.010	0.048	12936
J2137−1433	0.200	FOS	G130H-G190H	1	0.010	0.299	1	0.010	0.188	1191
J2138−3828	0.183	COS	G130M-G160M	1	0.010	0.283	1	0.010	0.171	12936
J2139−2454	0.939	STIS	G230L	1	0.933	1.039	1	—	—	8225
J2143+1743	0.213	FOS	G130H-G270H-G190H	1	0.010	0.312	1	0.010	0.200	1192
J2144−0754	1.811	STIS	G230L	1	1.116	1.606	0	—	—	9051
J2148+0657	0.999	FOS	G190H-G270H	1	0.369	1.098	1	0.369	0.979	2424
J2151+2130	1.534	STIS	G230L	1	0.724	1.605	0	—	—	8569
J2153−1514	0.078	STIS	G140L	1	0.047	0.177	2	0.047	0.067	9858
J2154−4414	0.344	COS	G130M-G160M	1	0.010	0.443	1	0.010	0.330	11541
		STIS	G140L	1	—	—	1	—	—	9506
J2155−0922	0.192	COS	G130M-G160M	1	0.010	0.291	1	0.010	0.180	12038
		STIS	G230L	1	—	—	1	—	—	9181
J2156+2242	1.290	COS	G160M	1	0.162	0.460	0	—	—	12593
J2158−3013	0.116	COS	G130M	1	0.010	0.209	1	0.010	0.104	12038
		FOS	G130H-G190H-G270H	1	0.210	0.215	1	—	—	1029,5089
J2159−2417	0.862	STIS	G230L	0	—	—	1	—	—	8225
J2203+3145	0.297	FOS	G130H-G190H-G270H	1	0.010	0.396	1	0.010	0.284	2578
J2211−1705	1.210	STIS	G230L	2	—	—	1	—	—	7359
J2215−2944	2.706	FOS	G270H	1	0.983	1.696	1	0.983	1.696	6093
		STIS	G230L	1	0.731	0.982	0	—	—	8569
J2217+1414	0.066	COS	G130M-G160M	1	0.010	0.166	1	0.010	0.055	12604
J2218−6150	0.000	STIS	G140L	0	—	—	1	—	—	8287
J2218−0335	0.901	FOS	G190H-G270H	1	0.587	1.000	1	0.587	0.882	2578,4052,5002
J2221−1857	0.000	STIS	G140L	0	—	—	1	—	—	8287
J2225−0456	1.404	FOS	G270H	1	1.018	1.503	1	1.018	1.380	2578
J2232+1143	1.037	FOS	G270H	1	0.839	1.136	1	0.839	1.016	2578
J2233−6033	2.238	STIS	G230L	1	0.010	1.598	1	0.010	1.598	7633,8076
J2236+1343	0.325	STIS	G230L	1	—	—	1	—	—	9507
J2242+2943	0.024	COS	G130M-G160M	1	0.010	0.124	1	0.010	0.014	12212
J2245−4652	0.198	COS	G130M-G160M	1	0.010	0.297	1	0.010	0.186	12604
J2246−1206	0.630	FOS	G190H-G270H	1	0.345	0.729	1	0.345	0.613	3791
		FOS	G160L	1	—	—	1	—	—	3791

Table 1 — *Continued*

QSO	z_{em} [a]	Instrument	Grating	Search Path			Statistical Path			Proposal ID
				F_{search} [b]	Min z	Max z	F_{stat} [c]	Min z	Max z	
J2248−5109	0.100	COS	G130M-G160M	1	0.010	0.199	1	0.010	0.089	11686
J2252−5021	2.900	STIS	G140L	0	—	—	1	—	—	8287
J2253−3658	3.200	STIS	G140L	0	—	—	1	—	—	8287
J2253+1608	0.859	COS	G130M-G160M	1	0.010	0.480	2	0.010	0.480	13398
		FOS	G190H-G270H	1	0.481	0.958	1	0.481	0.840	2578,6214
		FOS	G160L	1	—	—	1	—	—	2424
J2254−1734	0.068	COS	G130M-G160M	1	0.010	0.167	1	0.010	0.057	12029
		FOS	G130H-G190H-G270H	1	—	—	1	—	—	6484
J2254+1136	0.323	FOS	G130H-G190H-G270H	1	0.010	0.422	1	0.010	0.309	2424,2578,3791
J2255−5435	0.000	STIS	G140L	0	—	—	1	—	—	8287
J2257+1340	0.593	COS	G130M-G160M	1	0.010	0.476	2	0.010	0.476	11598
J2258−2758	0.926	STIS	G230L	1	0.379	1.026	1	0.379	0.907	8225
J2303+0852	0.015	COS	G130M-G160M	1	0.010	0.115	1	—	—	12212
J2303−6807	0.512	FOS	G190H-G270H	1	0.391	0.611	1	0.391	0.496	2424
		FOS	G160L	1	—	—	1	—	—	2424
J2304+0311	1.052	STIS	G140L	1	0.010	0.415	0	—	—	7358
J2311+1008	0.432	FOS	G270H-G190H-G130H	1	0.010	0.531	1	0.010	0.417	4079,4953
J2316−2849	0.000	STIS	G140L	0	—	—	1	—	—	8287
J2316−3349	3.100	STIS	G140L	0	—	—	1	—	—	8287
J2321−7026	0.300	COS	G130M-G160M	1	0.010	0.399	1	0.010	0.287	12936
J2328+0022	1.308	STIS	G230L	1	0.412	1.408	0	—	—	9382
J2330−5506	0.494	STIS	G230L	1	0.287	0.593	1	0.287	0.479	9507
J2331+0038	1.486	STIS	G230L	1	0.638	1.585	0	—	—	9382
J2334+0052	1.040	STIS	G230L	1	0.428	1.139	0	—	—	9382
J2339−0029	1.340	STIS	G230L	1	0.809	1.439	0	—	—	9382
J2342−0322	0.896	FOS	G190H-G270H	1	0.354	0.995	1	0.354	0.877	2424,4000
		FOS	G160L	1	—	—	1	—	—	4000
J2345−0059	0.789	COS	G130M-G160M	1	0.010	0.476	2	0.010	0.476	11598
J2345−1555	0.621	COS	G130M-G160M	1	0.010	0.480	0	—	—	13008
J2346−0016	3.504	STIS	G140L	0	—	—	1	—	—	9067
J2346+0930	0.672	FOS	G190H-G270H	1	0.354	0.771	1	0.354	0.655	3791
		FOS	G160L	1	—	—	1	—	—	3791
J2350−4325	2.885	COS	G130M	1	0.010	0.187	0	—	—	11528
		FOS	G270H-G190H	1	0.340	1.695	1	0.340	1.695	6449
		STIS	G230L	1	0.188	0.339	1	0.010	0.339	8875
J2351−1427	2.933	STIS	G140L	0	—	—	1	—	—	8287
J2351−0108	0.174	COS	G130M	1	0.010	0.209	1	0.010	0.162	12569
		FOS	G190H	1	—	—	1	—	—	4953
J2352−0028	1.624	STIS	G230L	2	—	—	0	—	—	9382
J2353−0028	0.761	STIS	G230L	1	0.483	0.860	0	—	—	9382
J2355−3357	0.702	FOS	G190H-G270H	1	0.346	0.801	1	0.346	0.685	2424
		FOS	G160L	1	—	—	1	—	—	2424
J2358−5440	0.000	STIS	G140L	0	—	—	1	—	—	8287
J2359−3037	0.165	COS	G130M	1	0.010	0.210	2	0.010	0.153	12864

[a] Emission redshift of quasar.

[b] Search flag: (0) Low S/N or bad spectrum; (1) Included; (2) BAL quasar.

[c] Statistical flag: (0) Non-Statistical; (1) Statistical; (2) Galaxy Sample.